Sustainable Energy, Grids and Networks 46 (2026) 102228

Contents lists available at ScienceDirect

Sustainable Energy, Grids and Networks

journal homepage: www.elsevier.com/locate/segan

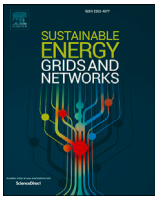

Power control of PV generation, flexible loads, and battery energy storage for frequency reserves provision☆

Sam Warmerdam, Nikolaos Damianakis*, Gautham Ram Chandra-Mouli

Technische Universiteit Delft (TU Delft), Faculty of Electrical Engineering, Mathematics, and Computer Science, Electrical Sustainable Energy Department, Mekelweg 4, 2628 CD Delft, the Netherlands

HIGHLIGHTS

- Providing aFRR by EVs and BESS on top of energy arbitrage yields double cost savings.
- EVs' contribution to ancillary services can become comparable to BESS in large grids.
- Higher potential for ancillary services for grids of diverse buildings and chargers.
- In contrast to solely energy arbitrage, V2G is highly used in ancillary services.
- Increasingly varied imbalance prices favor participation in the reserve market.

ARTICLE INFO

Keywords:
PV
Heat pumps
Electric vehicles
Battery energy storage
Automatic frequency restoration
Power control

ABSTRACT

Power control systems (PCSs) can exploit low-carbon technologies (LCTs) to provide grid ancillary services. This work develops a bilevel mixed-integer linear programming PCS of photovoltaics (PVs), electric vehicles (EVs), heat pumps (HPs), and battery energy storage systems (BESS), for providing automatic frequency restoration reserves (aFRR) with energy arbitrage, PV self-consumption, and customers' thermal and charging comfort. The contribution of the BESS and the flexible loads is evaluated under different seasons, grid types and sizes, and energy/reserve prices. Validating against a PCS solely for minimum grid energy cost (energy arbitrage), the findings demonstrate the increased cost savings when a PCS participates in the reserve market with BESS and EV combined. The cost of solely energy arbitrage was found consistently higher than 100% (e.g., 40*e* compared to only 19*e* with aFRR provision). These benefits have become more important recently in 2023, with the higher energy prices, and much higher reserve prices compared to 2018 (up to 540% increase). While the always present BESS is able to contribute more to ancillary services compared to the uncertain EV fleets, the contribution of EVs increased to a notable 38.5% of the total provided aFRR energy share at larger grids. Finally, mixed nodes that comprise both residential-commercial buildings and home-public chargers have a higher potential for ancillary services provision, demonstrating a 5x and 12x higher potential compared to residential and commercial nodes, respectively. Overall, this work highlights the importance of PCSs in large grids or with a variety of loads to provide ancillary services for enhanced savings.

1. Introduction

The European Union (EU) has set ambitious renewable energy targets under its REPowerEU program, aiming for a 42.5% share of renewable energy sources (RESs) by 2030, which would almost double the existing EU share of RESs [1]. The energy transition has led to heating and mobility electrification with heat pumps (HPs) and electric vehicles (EVs), respectively, and the abrupt increase of distributional energy resources (DERs), such as photovoltaics (PVs) [2]. For example, a total EV share increase among all passenger cars is noted in 2023, from 1.63% to 7.3%, as retrieved by the Rijksdienst voor Ondernemend Nederland database [3].

However, the rapid consumption electrification, e.g., of heating and mobility, already poses significant grid challenges [4]. For example, an increase in power peaks and load consumption was seen in [5,6],

☆ This study is funded by the Dutch Research Council (NWO) as part of the ongoing research project NEON.
* Corresponding author.
Email address: n.damianakis@tudelft.nl (N. Damianakis).

https://doi.org/10.1016/j.segan.2026.102228
Received 16 October 2025; Received in revised form 6 March 2026; Accepted 23 March 2026
Available online 24 March 2026

List of Acronyms

(B/H)ESS (Battery/Hybrid) Energy Storage System
(H)EMS (Home) Energy Management System
aFRR Automatic Frequency Restoration Reserves
BSP Balancing Service Provider
CC Constant-current
COP Coefficient of Performance
CV Constant-voltage
DA(M) Day-ahead Market
DER Distributed Energy Resource
DR Demand Response
DSO Distribution System Operator
EA Energy Arbitrage
EV Electric Vehicle
FCR Frequency Containment Reserves
HP Heat Pump
ISP Imbalance Settlement Period
LCOE Levelized Cost of Electricity
LCT Low-carbon Technology
LIB Lithium-ion Battery
MCS Monte Carlo Simulation
MILP Mixed-integer Linear Programming
PCS Power Control System
PDF Probability Distribution Function
PV Photovoltaics
RES Renewable Energy Source
RHO Receding Horizon Optimization
RT Real-time
SC Smart Charging
SOC State of Charge
TSO Transmission System Operator
V2G Vehicle-to-grid

respectively, while grid capacity reduction and congestion were noted in [7]. Grid congestion has also already been seen in the Netherlands, where some grid areas can no longer accept new connections. For instance, in 2023, the Dutch grid operator had 5600 requests for an electricity connection on a waiting list, resulting in significant delays in connecting new businesses and residential developments to the electricity grid [8]. Moreover, power quality issues and high voltage deviations were identified in [9], while overloading of components, such as transformers and cables, was reported in [10], which can also lead to extreme events, e.g., blackouts.

On the other hand, DERs, such as PVs, can provoke overvoltage and reverse power flows [4]. Moreover, RES generation is characterized by intermittency, which refers to the unpredictable fluctuations in the availability and reliability of RES, such as solar and wind power [11]. Furthermore, voltage flickering was observed in [12], and the voltage unbalance increase was seen in [13], since most of the LCTs, such as PVs, are single-phase connected. Overall, the high increase in electrical consumption and the RES generation intermittency have already become a major cause for larger grid frequency deviations, since they provoke higher net grid supply and demand mismatch [4]. Thus, grid ancillary services, such as frequency regulation provision, namely frequency containment reserves (FCR) and automatic frequency restoration reserves (aFRR), are increasingly needed to ensure grid stability and resilience [14,15]. Energy management systems (EMSs) (or power control systems, PCSs) that integrate RES generation (e.g., PVs) and exploit, firstly, the flexibility of loads, such as HPs and EVs with vehicle-to-grid (V2G) capabilities, and, secondly, energy storage systems (ESS) to provide ancillary services, become increasingly important [16–18]. For that reason, the studies in [19,20], and [21] have evaluated various ESS technologies, such as flywheels, supercapacitors, and battery ESS (BESS), e.g., lithium-ion batteries (LIBs), for their suitability in different PCS applications, such as supply-demand mismatch decrease, cost savings increase, peak shaving, etc. LIBs are favored for their high energy density, fast response time, and efficiency, though they still face cost challenges [19,20]. A schematic of such a grid-connected PCS that encompasses both residential and commercial buildings and exploits the flexibility of LCTs is depicted in Fig. 1.

It must be noted that in this work, the terms “power control systems (PCSs)” and EMSs are used interchangeably. Although most existing works prefer the term “EMS”, according to the authors’ opinion, the term “PCS” is more suitable since such systems mainly control power directly, and as a consequence, energy. Moreover, power control refers to the management of the power flows of the generation, consumption, and energy storage units and not to the power conversion sector.

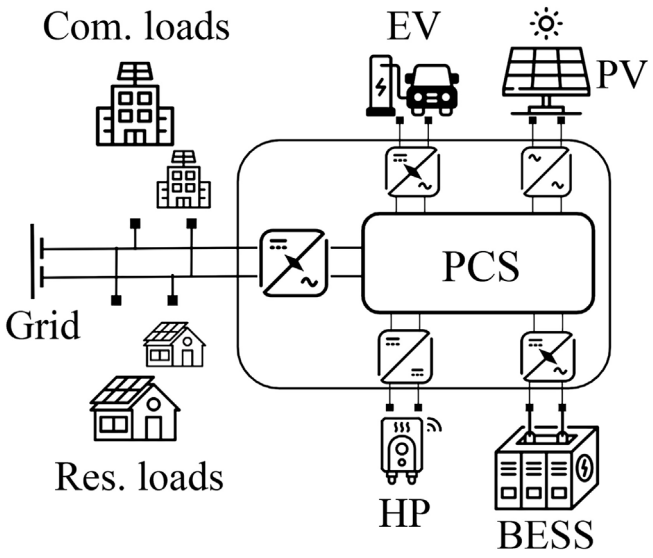

Fig. 1. Schematic of a grid-connected PCS that exploits the flexibility of LCTs to provide ancillary services.

2. Literature review

Several studies have developed PCSs to exploit flexible loads, such as EVs and HPs, and ESS for RES integration, cost savings, ancillary services, and other objectives.

2.1. PCSs: RES integration & energy arbitrage

The authors in [11] showed the potential of optimizing BESS use not only to increase cost savings, but also to cover PV generation intermittency; however, they did not consider the effect of residential loads that are present on the grid, such as in the PV-BESS systems of [22,23], and [24]. In [22], the integrated system was formulated as a Markov decision problem and was cost-optimized, accounting for the cost of battery life loss. The authors in [23] used a genetic algorithm to achieve a 17% reduction of voltage deviations together with cost optimization, while the authors in [24] aimed to optimize multiple objectives, such as energy and power autonomy, payback period, and capital costs. Additionally, the use of different hybrid ESS (HESS) types in EMSs is analyzed in [25,26] to show the benefits of using HESS over BESS for RES integration

and high-frequency loads coverage. While batteries and ultra-capacitors were found in [25] to effectively perform peak shaving, achieving a consistent 50% reduction of the peak load, they also limited frequency deviations in [26], maintaining the frequency nadir above 49 Hz. A particle swarm optimization algorithm has been employed in [27] to evaluate the impact of battery lifetime on the sizing of a similar HESS when high-frequency powers are provided by supercapacitors and low-frequency power by batteries for cost minimization. In addition, voltage control was combined with power optimization to maintain the voltage of the DC bus in the microgrid of [28] using different types of ESS. However, the above works studied the effect of ESS flexibility without considering flexible loads such as EVs and HPs.

Additionally, the use of EVs has been explored, either exploiting their V2G or load-shifting capabilities to enhance grid flexibility, dampen peak loads, and reduce operational costs. For example, the EV and V2G flexibility for day-ahead (DA) planning and maximum cost savings has been studied in [29,30]. For example, it was shown in [29] that EVs can be accommodated for all system users without increasing the grid peak load compared to the no-EV base case. Moreover, the EV V2G capabilities effectively allowed the EV fleets of [30] to participate in two-settlement markets, such as DA and real-time (RT) markets. However, RES and ESS integration was not taken into consideration. On the contrary, the benefits of the synergy between PV generation, EVs, and BESS, compared to the individual integration of LCTs for maximum use of the DA bought energy and minimum RT requests, were shown in [31] using a linear programming approach. Additionally, the same objective was studied in the decentralized approach of [32], imposing penalty costs on the deviated customers under different microgrid configurations.

Furthermore, the use of load-shifting capabilities of heating units, such as HPs, has also been studied in the literature and is missing from the above works. For example, the studies in [33,34] combined HPs with PV generation and BESS use in PCSs for building heating with RES exploitation and minimum cost. A combination of two-stage stochastic mixed-integer linear programming (MILP) and rule-based approaches was applied in [33] to achieve cost reduction under uncertain input conditions, while robust optimization was preferred in [34]. EVs were also included in the cost-optimization studies of [35,36]; a 4-stage chance constrained algorithm was used to optimize the DA, hour-ahead, and RT schedules in [35], while the authors in [36] focused on eliminating the peak period of EV charging.

Moreover, the integration of PVs, EVs, HPs, and ESSs in PCSs for self-consumption maximization was investigated in [37] for a building cluster in Sweden. It was also shown that the levelized cost of electricity (LCOE) can be notably decreased when EVs are utilized in RES-integrated power control systems. These findings are in agreement with the study in [38], which showed a 34% decrease in electricity cost by integrating PV, EV, HPs, and a BESS into a home EMS (HEMS). In addition, a similarly developed HEMS in [39] showed the significance of EV fleets for PV self-consumption increase. However, the developed EMSs in the aforementioned studies did not take into account the contribution and the revenues that can be gained in power control systems when ancillary services are also provided to the grid operator.

2.2. PCSs: ancillary services provision

Regarding the potential of PCSs to provide ancillary services to the grid operator, the cooperation of PVs with ESS and demand response (DR) incentive programs for prosumer participation in ancillaries has been explored in [40,41], and [42]. Their collective objective was to achieve maximum operational cost reduction, taking advantage of the revenues from ancillary services provision, which succeeded in all the investigated DR programs. For example, model predictive approaches were shown in [40] to achieve a 23.47% cost reduction compared to logic-based control when the EMS participated in ancillary services. Moreover, incentive-based services, such as emergency DR and direct load control, were found to be superior to price-based tariffs for cost-reduction in [41], while the use of ESS as a transient power supply during sudden load changes was investigated in [42].

However, the studies did not consider the contribution of flexible loads, such as EVs and HPs. EVs were incorporated with PVs and BESS in the component sizing and power optimization study of [43], aiming for simultaneous cost and FCR provision optimization. Moreover, the authors in [44] conducted a sizing and power optimization analysis utilizing an HESS and aiming for PV self-consumption maximization and optimal cost via participation in the FCR market. However, the benefits of the synergy with HPs were not taken into consideration. On the contrary, the authors in [45] showed that the control of HPs together with ESS, RES, and EVs in DR programs can greatly enhance the EMS flexibility for energy arbitrage and ancillary services provision. However, the work in [45] investigated only the cooperative flexibility of the assets and did not proceed to comparisons regarding their individual contribution. Moreover, all of the studies in this section focused on primary frequency regulation (FCR) and not on secondary (aFRR).

On the contrary, the BESS participation in multiple energy markets (FCR, aFRR, etc.) was studied in [46–48], aiming to quantify the potential of stacked revenue. In [46], a state-of-charge (SOC) supervision and regulation was studied via a local controller to avoid the provision of scheduled power beyond the battery's SOC limits. It was found that a BESS can effectively emulate inertial response and provide FCR followed by aFRR while maintaining the SOC within acceptable variation limits. Moreover, the revenues by a joint participation in energy and reserve markets showed a 76% increase in the annual profits in [47], while voltage variations and congestion issues were also mitigated in [48] by combined FCR and peak-shaving provision. Overall, each study showed a significant increase in revenue, indicating the BESS potential to operate in multiple energy markets. However, the study in [47] did not consider RES and smart loads integration, while the authors in [47,48] only included the effect of PV generation in their studies.

3. Contributions

As can be observed in Table 1, multiple grid-level power control works in the literature have explored the integration of RESs with flexible loads and/or ESS to provide flexibility for cost benefits, ancillary services provision, or other objectives in PCSs. However, a multi-objective PCS that integrates PVs, HPs, EVs with V2G capabilities, and BESS and aims to optimize the energy arbitrage cost and revenues by ancillary services provision while respecting the customers' comfort and grid limits is still missing. Moreover, according to the author's knowledge, the potential of ancillary services provision (such as aFRR) by BESS and flexible loads such as V2G-capable EVs has not yet been investigated and compared under different influencing factors, such as seasons, grid types, grid sizes, and energy prices in the existing literature. Hence, the contributions of this work can be summarized as follows.

- Develops a bi-level MILP power control model that encompasses and optimizes PV generation, EVs, HPs, and BESS for energy arbitrage and aFRR reserves provision, achieving maximum cost savings while respecting grid power limits and ensuring customers' charging and thermal comfort.
- Investigates and compares the performance of EVs and BESS concerning energy arbitrage and aFRR provision, modeling in detail the imbalance market and accounting for multiple influencing factors, namely different grid types, seasons, and energy prices.
- Applies the developed power control model in two different grid size scenarios, a small (3-node) grid and a large (13-node) grid, demonstrating the scalability of the model and validating the performance of EVs and BESS on aFRR provision at a real grid level.

This work can provide distribution system operators (DSOs) with valuable insights into the individual and cooperative potential of BESS and EV chargers to establish a more flexible and frequency-balanced

Table 1
Summary of characteristics & Contributions of grid-level Cost-oriented power control studies.

Studies	RES	HPs	EVs	V2G	ESS	Ancillary Services	ESS vs RES/ Flexible loads	Seasonal/ Meteorological effect	Energy price/ Reserve price effect	Grid-type effect	Grid-size effect
[22]	✓(PVs)				✓(BESS)						
[27]	✓(PVs)				✓(BESS)			✓			
[23]	✓(PVs)				✓(BESS)			✓	✓		
[24]	✓(PVs)				✓(BESS)			✓	✓		
[31]	✓		✓	✓	✓		✓				
[32]	✓(PVs)		✓	✓	✓(BESS)						✓
[33]	✓(PVs)	✓			✓(BESS)			✓	✓		
[37]	✓(PVs)	✓	✓	✓	✓		✓	✓			✓
[47]					✓(BESS)	✓(aFRR)		✓			
[42]	✓(PVs)				✓	✓			✓		
[11]	✓(PVs)				✓(BESS)	✓		✓	✓		
[41]	✓(PVs)				✓(BESS)	✓			✓	✓	✓
[46]	✓(PVs)				✓(BESS)	✓(aFRR)	✓				
[48]	✓(PVs)				✓(BESS)	✓(aFRR)	✓	✓	✓		
[40]	✓(PVs)				✓(BESS)	✓(aFRR)		✓	✓		
[45]	✓	✓	✓		✓	✓		✓			
[35]	✓(PVs)		✓	✓	✓(BESS)	✓			✓		
[43]	✓(PVs)		✓	✓	✓(BESS)	✓		✓			
Work	✓(PVs)	✓	✓	✓	✓(BESS)	✓(aFRR)	✓	✓	✓	✓	✓

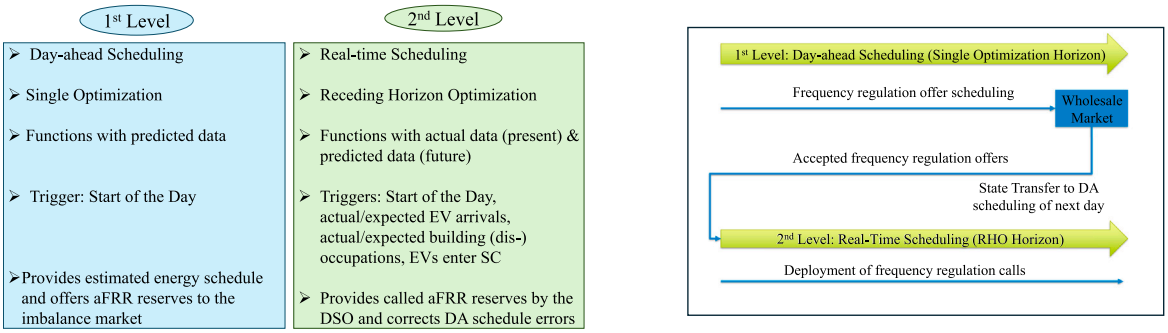

(a) Functionalities of Levels 1 and 2 of the PCS model.

(b) Use of Levels 1 and 2 for participation in the imbalance market.

Fig. 2. Description of the PCS concept for energy arbitrage and aFRR provision.

power grid through effective participation in the imbalance market, while also considering various uncertain influencing factors.

4. Power control concept

The PCS comprises a number of entities that constitute aggregated EV chargers and buildings (here and onwards called nodes) and controls them distributionally. Each building has a residential or commercial load, depending on the type of building, and is equipped with a PV rooftop and an HP, while each node also comprises a BESS. Finally, every node communicates with the main grid for grid power exchange and aFRR provision. Both EVs with V2G and BESS participate in aFRR services to provide balancing services to the main grid and decrease the total node power control cost. The PCS model is based on [49], but in this work, it is formulated as a bi-level MILP problem for DA and RT scheduling. Every level is fed with information about the weather, EV fleet patterns, buildings' occupancy, and price data from the energy and reserves markets. Since the PCS is handled by the aggregators, the optimization is formulated by the aggregator's point of view, which uses the aforementioned assets (flexible loads and BESS) to bid in both wholesale energy and reserve markets.

As Fig. 2(a) depicts, Level 1 uses a single (or one-shot) optimization, is triggered at the start of the day, and uses predicted data about the building occupancy and the EV driving patterns (arrival SOCs, requested amounts of energy, arrival and departure times, EV characteristics, etc.). Moreover, it provides the estimated energy scheduling and offers aFRR reserves to the wholesale market, as seen in Fig. 2(b). On the contrary, Level 2 uses a receding horizon optimization (RHO), and is triggered upon several events, such as the start of the day, actual/expected EV arrivals, actual/expected building (dis-)occupancies, and when EVs enter smart-charging (SC), which occurs when $SOC > 20\%$. With the use of RHO and re-optimizations, Level 2 being fed with the actual data of building occupation and EV driving patterns continuously during the horizon, it corrects the accuracy errors between the actual and predicted data with re-optimizations, providing uncertainty management. Finally, it provides the called amount of aFRR reserves for deployment that have been accepted in the wholesale market (Fig. 2(b)). The horizon of both levels ends at the end of the day or the latest departure of the connected EVs at that time instant.

It must be noted that the actual and predicted building occupancy changes, as well as EV arrival and departure times have a maximum accuracy error of $15'$. That means that if an EV has informed the EV charger of an arrival time at 8:00, we assume that it will arrive between 7:45 and 8:15. This uncertainty set has been derived by [50], where most EV arrivals are clustered within a 30-minute window around the estimated arrival time. Moreover, spot energy and reserve markets function at 15-minute products, allowing EV chargers to trade flexibility and adjust to arrival deviations in real-time [51]. Hence, a deviation of $\pm$ one 15-minute block has been considered appropriate for a study of grid ancillary services. While higher uncertainties have not been studied in this work, the impact of parking time uncertainty (arrival and departure) on power control has been thoroughly investigated in our previous work [52], where the reader is referred for further information.

5. Power control modeling

This section comprises the modeling of the bi-level PCS model and is categorized into the EV and BESS, building, imbalance market, node constraints, and the objective function. The indices $n, j, bes, T, ch, dis, init, fr, u, d, \Delta t$ represent the node, charger, BESS, optimization horizon, charging, and discharging, initial, aFRR, up, down, and the timestep equal to 5′ respectively. The aFRR modeling is based on the work in [53]. The proposed power control model simulates participation in the Dutch aFRR market, operated by TenneT under the EEBG (European Electricity Balancing Guideline). Each flexible asset capable of providing aFRR participates individually, submitting and delivering aFRR capacity as if it were a balance service provider (BSP). The energy schedule and aFRR capacity offer per ISP are scheduled day-ahead (Level 1), while the accepted capacity is automatically activated by the TSO real-time (Level 2), with deployment modelled probabilistically and without partial activation. Electricity consumption and injection are settled using hourly day-ahead wholesale prices, uniform across all nodes, while taxes, levies, and network tariffs are excluded to preserve the general applicability of the model, and node-level import/export limits represent distribution grid constraints. As a result, the reported cost outcomes represent marginal wholesale energy costs rather than final prosumer electricity bills.

5.1. EV & BESS constraints

In this section, the EV and BESS modeling is described. It must be noted that the variables written in bold letters with a "*" constitute the variables that are transferred as parameters from the DA Level 1 to the RT Level 2. Moreover, the equations in red-colored parentheses with a "*" are only integrated into Level 1.

$$\begin{aligned} P^{n,j/bes,t}_{ch/dis} &= \Phi^{n,j} I^{n,j/bes,t}_{ch/dis} V^{n,t} \quad \forall t \in T \\ \mathbf{P^{n,j/bes,t^*}_{fr_u/fr_d}} &= \Phi^{n,j} I^{n,j/bes,t}_{fr_u/fr_d} V^{n,t} \quad \forall t \in T \end{aligned} \tag{1}$$

$$\begin{aligned} B^{n,j/bes,t} = B^{n,j/bes}_{init} + \Delta t \sum_{t_{init}}^{t} \left(P^{n,j/bes,t}_{ch} - P^{n,j/bes,t}_{dis} \right) \\ + \Delta t \sum_{t_{init}}^{t} \left(\mathbf{P^{n,j/bes,t^*}_{fr_d}} h^{n,j}_{ch/bes} - \frac{\mathbf{P^{n,j/bes,t^*}_{fr_u}}}{h^{n,j}_{ch/bes}} \right) \quad \forall t \in T \end{aligned} \tag{2}$$

$$S^{n,j/bes,t} = \frac{B^{n,j/bes,t}}{B^{n,j/bes}_{r}} \quad \forall t \in T \tag{3}$$

Equations in (1) model the EV and BESS charging, discharging, up aFRR, and down aFRR powers $P^{n,j,t}_{ch/dis/fr_u/fr_d}$ & $P^{n,bes,t}_{ch/dis/fr_u/fr_d}$ which depend on the number of phases $\Phi^{n,j}$ equal to 3, the node voltage $V^{n,t}$ steady at 230 V, and the charging/discharging/up aFRR/down aFRR currents $I^{n,j,t}_{ch/dis/fr_u/fr_d}$ & $I^{n,bes,t}_{ch/dis/fr_u/fr_d}$. Moreover, (2) & (3) dictate the battery capacity B and SOC S dynamics of the EVs and the BESS. The EV and BESS battery capacities depend on the initial capacity B_{init} (equal to the arrival capacity $B^{n,j}_{a}$ for the EVs and 50% for the BESS), and the sum of the charging, discharging, and aFRR power amounts from the initial time t_{init} (arrival time $T^{n,j}_{a}$ for the EVs or the start of the simulation for the BESS). Moreover, the BESS and EV SOCs S depend on the dynamic battery capacities B divided by the rated capacity B_r. It must be noted that charging and discharging powers are measured at the EVs and BESS while aFRR powers are measured at the connection point with the main grid, and hence, they are integrated with the (dis)charging efficiency $h^{n,j}_{ch}, h^{n}_{bes}$ which comprise the power losses of both the charger and the EV battery management system.

$$\begin{aligned} P^{n,j/bes,t}_{ch} + \mathbf{P^{n,j/bes,t^*}_{fr_d}} h^{n,j}_{ch/bes} \le \left(\frac{S^{n,j/bes,t}}{k} + \frac{\alpha k - \beta}{\alpha k} \right) P^{n,j/bes}_{ch_{max}} \\ \alpha = 10, \beta = 9, k = 16 \; \forall t \in T \end{aligned} \tag{4}$$

$$\begin{aligned} I^{n,j/bes,t}_{ch} + I^{n,j/bes,t}_{fr_d} h^{n,j}_{ch/bes} \le I^{n,j/bes,t}_{cv_{max,ch}} \quad \forall t \in T \\ I^{n,j/bes,t}_{cv_{max,ch}} = -\gamma I^{n,j/bes,t}_{r} S^{n,j/bes,t} + \gamma I^{n,j/bes,t}_{r} \end{aligned} \tag{5}$$

$$\begin{aligned} I^{n,j/bes,t}_{dis} + \frac{I^{n,j/bes,t}_{fr_u}}{h^{n,j}_{ch/bes}} \le I^{n,j/bes,t}_{cv_{max,dis}} \quad \forall t \in T \\ I^{n,j/bes,t}_{cv_{max,dis}} = \gamma I^{n,j/bes,t}_{r} S^{n,j/bes,t} \end{aligned} \tag{6}$$

Eqs. (4)–(6) constitute a linear representation of the constant-current (CC) and constant-voltage (CV) regions for charging and discharging. Concerning (4)-(5) and charging, using the defined α, β, k, γ the limit of the sum of charging and down aFRR powers increases linearly up to $SOC = 90\%$, where it reaches the rated BESS and EV power $P^{n,j/bes}_{ch_{max}}$, and thereafter, it decreases linearly to zero when $SOC = 100\%$. The latter is dictated by the maximum current variables $I^{n,j/bes,t}_{cv_{max,ch}}$ which depend on the EV and BESS SOC and rated currents I_r. Similarly, concerning (6) and discharging, the limit of the sum of discharging and up aFRR powers increases linearly to the maximum value (rated power) when $SOC = [0\%, 10\%]$ (dictated in the same manner by the maximum current variables $I^{n,j/bes,t}_{cv_{dis}}$, and then remains steady when $SOC = [10\%, 100\%]$.

$$b^{n,j/bes,t}_{ch} + b^{n,j/bes,t}_{dis} \le 1 \quad \forall t \in T \tag{7}$$

$$\left(b^{n,j/bes,t}_{fr_u} + b^{n,j/bes,t}_{fr_d} \le 1 \quad \forall t \in T \right)^{*} \tag{8}$$

$$\mathbf{b^{n,j/bes,t^*}_{fr_u}} + b^{n,j/bes,t}_{ch} \le 1 \quad \forall t \in T \tag{9}$$

$$\mathbf{b^{n,j/bes,t^*}_{fr_d}} + b^{n,j/bes,t}_{dis} \le 1 \quad \forall t \in T \tag{10}$$

$$P^{n,j/bes,t}_{ch} \le b^{n,j/bes,t}_{ch} P^{n,j/bes}_{ch_{max}} \quad \forall t \in T \tag{11}$$

$$P^{n,j/bes,t}_{dis} \le b^{n,j/bes,t}_{dis} P^{n,j/bes}_{dis_{max}} \quad \forall t \in T \tag{12}$$

$$\left(P^{n,j/bes,t}_{fr_u} \le b^{n,j/bes,t}_{fr_u} P^{n,j/bes}_{dis_{max}} \quad \forall t \in T \right)^{*} \tag{13}$$

$$\left(P^{n,j/bes,t}_{fr_d} \le b^{n,j/bes,t}_{fr_d} P^{n,j/bes}_{ch_{max}} \quad \forall t \in T \right)^{*} \tag{14}$$

Moreover, four binary variables $b_{ch}, b_{dis}, b_{fr_d}, b_{fr_u}$ are utilized in (7)–(10) for $P_{ch}, P_{dis}, P_{fr_d}, P_{fr_u}$, respectively, which together with (11)–(14) limit the maximum power values and enforce that only the pairs P_{ch}, P_{fr_d} and P_{dis}, P_{fr_u} can occur simultaneously for both EVs and BESS, where $P_{ch_{max}}$ & $P_{dis_{max}}$ are the maximum charging and discharging power, respectively.

$$I^{n,j,t}_{ch/dis}, I^{n,j,t}_{fr_u/fr_d}, b^{n,j,t}_{ch/dis}, \left(b^{n,j,t}_{fr_u/fr_d} \right)^{*} = 0 \quad \forall t \notin [T^{n,j}_{a}, T^{n,j}_{d}] \tag{15}$$

$$E^{n,j}_{g} = B^{n,j}_{a} + d^{n,j} - B^{n,j}_{d} \tag{16}$$

Finally, (15) sets the EV charging, discharging, up-aFRR, and down-aFRR currents $I_{ch}, I_{dis}, I_{fr_u}, I_{fr_d}$ and binary variables to zero outside of the EV parking time $[T^{n,j}_{a}, T^{n,j}_{d}]$. Moreover, (16) calculates the EV unfinished charging gap $E^{n,j}_{g}$ which is the subtraction of the departure EV battery energy $B^{n,j}_{d}$ from the sum of the arrival energy $B^{n,j}_{a}$ and the requested energy $d^{n,j}$. A penalty cost is inflicted on the power control system for every EV unfinished charging kWh, which is used in the objective function.

5.2. Building constraints

In this section, a summary of the building constraints from [49, 54] is described for the control of the PV rooftop generation and

HP heating/cooling, where b, sf, irr denote the building, surface, and irradiation, respectively. All the following constraints apply for $\forall t \in T$.

$$T^{n,b,t} = T^{n,b}_{init} + \Delta t \sum_{t_{st}}^{t} \frac{Q^{n,b,t}_{tot}}{C_b + V_b C_{air} \rho_{air}} \tag{17}$$

$$Q^{n,b,t}_{tot} = Q^{n,b,t}_{hp} m^{n,b} + I^{n,b,t}_{r} - \left(\sum_{sf} U_{sf} A_{sf} + C_{air}\ \rho_{air}\ r_b \right) (T^{n,b,t} - T^{t}_{a}) \tag{18}$$

$$P^{n,b,t}_{hp} = \frac{Q^{n,b,t}_{hp}}{c^{n,b,t}_{p_{hp}}} \tag{19}$$

Concerning the building equations, (17) dictates the dynamics of the buildings' temperature T which depends on the sum of heating losses and gains Q_{tot} divided by the total building thermal capacity (the capacity of the building structure C_b and of the total air inside) and the initial building temperature at the start of the simulation T_{init}, where V_b, C_{air}, and ρ_{air} the building volume, air thermal capacity, and air density, respectively. Moreover, (18) dictates that Q_{tot} comprises the heating gains by the HP Q_{hp} and solar irradiation I_r, and the conductive and ventilation losses, which depend on the temperature difference between the building and ambient air T_a. U_{sf}, A_{sf}, and r_b represent the conductivity and acreage of every surface and air change rate of the building, respectively. Furthermore, the variable m controls the operation of the HP and is equal to $+1$ for heating and -1 for cooling. Eq. (19) dictates the relation between the HP power P_{hp}, heating output Q_{hp}, and coefficient of performance (COP) $c_{p_{hp}}$, assumed steady.

$$P^{n,b,t}_{pv_{dev}} = P^{n,b,t}_{pv_{max}} - P^{n,b,t}_{pv_{use}} \text{ where } 0 \le P^{n,b,t}_{pv_{use}} \le P^{n,b,t}_{pv_{max}} \tag{20}$$

$$\begin{aligned} T^{n,b,t}_{dev} &= \max(T^{n,b,t} - T^{n,b}_{high}, T^{n,b}_{low} - T^{n,b,t}, 0) \Leftrightarrow \\ T^{n,b,t}_{dev} &= \max(\max(T^{n,b,t} - T^{n,b}_{high}, T^{n,b}_{low} - T^{n,b,t}), 0) \end{aligned} \tag{21}$$

Additionally, (20) calculates the PV power deviation $P_{pv_{dev}}$ between the PV generated power $P_{pv_{max}}$ and the used PV power $P_{pv_{use}}$ which the model aims to minimize to zero for maximum self-sufficiency (see Section 5.5). Finally, (21) calculates the distance of the building temperature from the desired temperature range $[T_{low}, T_{high}]$, which in this work has been assumed to be [21,23]. The calculation has been modeled with the use of two max functions and outputs zero if the building temperature is inside the range. For the integration of (21) in the MILP model, the reader is referred to [49].

5.3. Imbalance market constraints

This section describes some further constraints which dictate the imbalance market norms and the participation of the PCS; hence, the bidding and scheduling of aFRR reserves to the market in DA and their deployment in RT when called by the transmission system operator (TSO). The indices $park, da, rt, a, d, isp$ denote the parking time, day-ahead, real-time, arrival, departure, and imbalance settlement period (ISP), respectively.

5.3.1. Day-ahead (Level 1)

$$\begin{aligned} &\text{if } \Delta T^{n,j}_{park-da} = [T^{n,j}_{a-da} : T^{n,j}_{d-da}] \rightarrow \\ &\quad \Delta T^{n,j}_{park-rt} = [T^{n,j}_{a-rt} : T^{n,j}_{d-rt}] \text{ where:} \\ &\quad T^{n,j}_{a-rt} = T^{n,j}_{a-da} + \delta \quad \& \quad T^{n,j}_{d-rt} = T^{d,j}_{a-da} + \delta : \\ &\qquad -K \le \delta \le K \quad \& \quad K = 15' \end{aligned} \tag{22}$$

To account for the uncertainty considered in the arrival and departure times of the EV fleets, (22) dictates that the real-time EV parking time $\Delta T^{n,j}_{park-rt}$ in Level 2 deviates from the estimated parking time in day-ahead $\Delta T^{n,j}_{park-da}$ by a time difference δ of maximum $K = 15'$ considered in both the arrival and departure times $T^{n,j}_{a} : T^{n,j}_{d}$, respectively. This is because the parking time uncertainty needs to be considered in the aFRR bidding from EVs in DA; hence, the EVs are only allowed to offer aFRR during the parking time $[T^{n,j}_{a-da} + |K|, T^{n,j}_{d-da} - |K|]$ to ensure that the EV will be present to deploy the called reserves in RT. Hence, δ is an exogenous random parameter, unknown to Level 1, whose maximum value K is considered in the estimated scheduling to offer robustly aFRR reserves.

$$\begin{aligned} b^{n,bes,t}_{fr_{u/d}} &= b^{isp}_{up/down}\ \forall isp \in T \\ b^{n,j,t}_{fr_{u/d}} &= b^{isp}_{up/down}\ \forall isp \in \Delta T^{n,j}_{park-rt}\ \&\ ISP = 15 \\ \text{where}: \ l_{isp} &= \frac{ISP = 15'}{\Delta t = 5'} \end{aligned} \tag{23}$$

$$\begin{aligned} b^{isp}_{up} = 1 \Rightarrow P^{n,j/bes,t}_{fr_u} = P^{n,j/bes,t+1}_{fr_u},\ \forall isp^{j/bes} \\ b^{isp}_{down} = 1 \Rightarrow P^{n,j/bes,t}_{fr_d} = P^{n,j/bes,t+1}_{fr_d},\ \forall isp^{j/bes} \end{aligned} \tag{24}$$

Moreover, (23) and (24) enforce that the aFRR bidding of the power control model respects the norms of the wholesale reserve market. The time horizon T of the power control is divided into consecutive ISPs that end for $15'$, the number of which is defined by $T//l_{isp}$. The PCS model acting as a BSP is obligated to offer the same amount of up or down aFRR reserves for 15 consecutive minutes (the whole ISP) according to the rules of the aFRR market. Hence, up and down binary variables, $b^{isp}_{up}, b^{isp}_{down}$ respectively, are introduced for all the ISP blocks which are equal to the up and down aFRR binary variables, $b^{n,j/bes,t}_{fr_u}, b^{n,j/bes,t}_{fr_d}$ for the BESS and EVs. Concerning the BESS, this is enforced for the whole horizon T, while for the EVs, it is enforced for the estimated minimum parking time in real-time $\Delta T^{n,j}_{park-rt}$. Eq. (23) ensures, with the use of the binaries, that the bidding remains the same for the whole ISP, while (24) dictates that for every timestep t in the ISP, the scheduled EV/BESS up and down aFRR power must be the same as the scheduled amounts at the consecutive timestep $t+1$ in the same ISP. In simpler terms, this ensures that the power remains constant over the bidding interval determined by the ISP, according to market rules set by the TSO.

It needs to be clarified that two forms of partial aFRR activation exist. Partial activation within an imbalance settlement period is explicitly modelled using activation parameters derived from historical Dutch aFRR data. However, partial acceptance of offered aFRR capacity due to limited system-wide reserve demand or market-clearing competition is not modelled, as bids are assumed to be fully accepted. Consequently, system-level aFRR procurement dynamics are only partially represented.

5.3.2. Real-time (Level 2)

$$\begin{aligned} P_r\left(P^{n,j/bes,t}_{fr_u-rt} = P^{n,j/bes,t}_{fr_u-da}\right) &= \alpha_{up} \\ P_r\left(P^{n,j/bes,t}_{fr_d-rt} = P^{n,j/bes,t}_{fr_d-da}\right) &= \alpha_{down} \\ P_r\left(P^{n,j/bes,t}_{fr_u-rt} = 0 \mid P^{n,j/bes,t}_{fr_u-da}\right) &= 1 - \alpha_{up} \\ P_r\left(P^{n,j/bes,t}_{fr_d-rt} = 0 \mid P^{n,j/bes,t}_{fr_d-da}\right) &= 1 - \alpha_{down} \end{aligned} \tag{25}$$

Where:

- α_{up} and α_{down} are the probabilities that the DA offered up and down aFRR reserves to the market (Level 1) remain equal to the called up and down aFRR reserves from the TSO in RT, respectively (Level 2).
- $1 - \alpha_{up}$ and $1 - \alpha_{down}$ are the probabilities that the called up and down aFRR reserves in real-time are zero. In this work, as explained below, only these two possibilities are considered.

Finally, 4 different variables are transferred from Level 1 to Level 2: the up and down binary variables $b^{n,j/bes,t}_{fr_{u/d}}$ and the up and down aFRR powers $P^{n,j/bes,t}_{fr_{u/d}}$. The binary variables are transferred as is; however, the scheduled power amounts $P^{n,j/bes,t}_{fr_{u/d}-da}$ deviate from the deployed $P^{n,j/bes,t}_{fr_{u/d}-rt}$ due to acceptance and deployment rates. In this work, it has been assumed that all offered aFRR reserves are accepted as a whole in the wholesale market, because the PCS is allowed to participate with zero bids in the market since the aFRR reserves come from RESs. Thus, the bidding of the power control model is always below the market-clearing price. However, when aFRR power is called by the TSO during a certain ISP, it is not uniform throughout the full delivery period. For example, an upward power request from the TSO can be positive during the first ten minutes of an ISP and zero during the last five. Therefore, aFRR deployment rates for upward and downward power requests are introduced, denoted as α_{up} and α_{down}. These rates represent the chance that scheduled aFRR power is actually called during a timestep in the simulation. By using these rates, a more realistic version of the potential voluntary aFRR earnings is approached. Calculated from 2023 TenneT aFRR data [55], the average upward and downward activation percentages per ISP are 71% and 41%, respectively. These rates are integrated into the power control model with the use of (25).

5.4. Node constraints

The node constraints, which constitute the node power balance, and the grid input and output power limits are included here. All the node constraints apply for $\forall t \in T$.

$$P^{n,t}_{im} - P^{n,t}_{ex} = \sum_{j=1}^{J}\left(\frac{P^{n,j,t}_{ch}}{h^{n,j}_{ch}} - P^{n,j,t}_{dis}h^{n,j}_{ch}\right) + \frac{P^{n,bes,t}_{ch}}{h^{n}_{bes}} - P^{n,bes,t}_{dis}h^{n}_{bes} + \sum_{b=1}^{B}\left(P^{n,b,t}_{hp} + P^{n,b,t}_{l} - P^{n,b,t}_{pv}\right),\ \forall t \in T \tag{26}$$

$$\sum_{j=1}^{J}\left(\frac{P^{n,j,t}_{ch}}{h^{n,j}_{ch}} - P^{n,j,t}_{dis}h^{n,j}_{ch}\right) + \frac{P^{n,bes,t}_{ch}}{h^{n}_{bes}} - P^{n,bes,t}_{dis}h^{n}_{bes} + \sum_{b=1}^{B}(P^{n,b,t}_{hp} + P^{n,b,t}_{l} - P^{n,b,t}_{pv}) + \sum_{j=1}^{J}\mathbf{P^{n,j,t^*}_{fr_d}} + \mathbf{P^{n,bes,t^*}_{fr_d}} - \sum_{j=1}^{J}\mathbf{P^{n,j,t^*}_{fr_u}} - \mathbf{P^{n,bes,t^*}_{fr_u}} \le G^{n}_{in},\ \forall t \in T \tag{27}$$

$$\sum_{j=1}^{J}\left(P^{n,j,t}_{dis}h^{n,j}_{ch} - \frac{P^{n,j,t}_{ch}}{h^{n,j}_{ch}}\right) - \frac{P^{n,bes,t}_{ch}}{h^{n}_{bes}} + P^{n,bes,t}_{dis}h^{n}_{bes} - \sum_{b=1}^{B}(P^{n,b,t}_{hp} + P^{n,b,t}_{l} - P^{n,b,t}_{pv}) - \sum_{j=1}^{J}\mathbf{P^{n,j,t^*}_{fr_d}} - \mathbf{P^{n,bes,t}_{fr_d}} + \sum_{j=1}^{J}\mathbf{P^{n,j,t^*}_{fr_u}} + \mathbf{P^{n,bes,t^*}_{fr_u}} \le G^{n}_{out},\ \forall t \in T \tag{28}$$

Eq. (26) constitutes the power balance of the node and dictates that the total imported grid power P_{im} is the sum of EV and BESS charging power and the sum of building power consumption for heating/cooling and base load cover (P_l) at every timestep. On the contrary, the total exported grid power P_{ex} is the sum of the EV and BESS discharging power and the building PV generation. Moreover, (27) forces the total imported power and EV/BESS down aFRR provision to comply with the imported power limit G_{in}, while (28) forces the total exported power and up aFRR provision to be below the exported power limit G_{out}. The formulation of (26)–(28) also enforces that the node only imports or exports grid power at every timestep. Finally, the EV and BESS up and down aFRR powers are only integrated into the input and output grid limit equations and not in the power balance. This is because, for example, if down aFRR was contained in (26), the node would buy imported power to cover the down aFRR, which is provided as an ancillary service to the main grid for revenues. Hence, aFRR reserves are only integrated into the grid limit equations to reduce the input and output limits for the optimization of the rest of the system, which must always respect the power balance.

5.5. Objective function

Eq. (29) is the objective function of the PCS which is a multi-objective problem, whose objectives have been translated into a total cost C_n aimed to be minimized.

$$\begin{aligned}\min C_n = \Delta t\Bigg(&\sum_{t=1}^{T}\left(P^{n,t}_{im}C^{t}_{buy} - P^{n,t}_{ex}C^{t}_{sell}\right) + \sum_{t=1}^{T}\sum_{b=1}^{B}\left(P^{n,b,t}_{pv_{dev}}C^{n,b}_{pv_{pen}}\right) + \sum_{t=1}^{T}\sum_{b=1}^{B}\left(T^{n,b,t}_{dev}C^{n,b}_{hp_{pen}}O^{t,n,b}\right)\\ &\Bigg(+\sum_{t=1}^{T}\left(\sum_{j=1}^{J}\left(P^{n,j,t}_{fr_d}\right) + P^{n,bes,t}_{fr_d}\right)C^{t}_{down} - \sum_{t=1}^{T}\left(\sum_{j=1}^{J}(P^{n,j,t}_{fr_u}) + P^{n,bes,t}_{fr_u}\right)C^{t}_{up}\Bigg)\Bigg)^{*} + \sum_{j=1}^{J}E^{n,j}_{g}C^{n,j}_{ev_{pen}}\end{aligned} \tag{29}$$

Term 1) Energy arbitrage: The PCS aims to exchange power with the grid with minimum imported power cost and maximum exported cost, where C_{buy}, C_{sell} are the respective DA energy costs.

Term 2) Maximum PV self-consumption: The PCS is inflicted with a PV curtailment cost, where $C_{pv_{pen}}$ is the related penalty.

Term 3) Respect of the buildings' thermal comfort: The PCS aims to keep the buildings' temperature always within the desired temperature interval and is burdened with a thermal discomfort penalty $C_{hp_{pen}}$ when there is a temperature deviation. Moreover, this objective function term comprises the building occupancy (0 or 1)] $O^{t,n,b}$, dictating that no thermal discomfort penalty should be placed if the building is not occupied.

Term 4) Maximum earnings from aFRR provision from the EV fleets and BESS, where C_{up} and C_{down} are the reserve prices of up and down regulation in the imbalance market, respectively. It must be noted that in the aFRR market, the BSPs are remunerated for both what they offer in DA and what they deliver in RT, in contrast with FCR, where they are remunerated only for what they offer; hence, for the available capacity. However, this term is only integrated into the objective function of Level 1 during the scheduling of the offered aFRR reserves and not into Level 2. This is because the PCS seeks to maximize its earnings during the DA scheduling, offering the highest reserves, while the called reserves in RT are only controlled by the TSO.

Term 5) Respect of the EVs' charging demand: A cost penalty $C_{pv_{pen}}$ is inflicted for the total EV unfinished charging gap, which is measured in e/kWh.

Fig. 3 depicts the equations of Level 1 that are used, not used, and modified in Level 2, and the variables that are transferred as parameters between the two levels. Furthermore, Tables 2 and 3 comprise the parameters used in the EV/BESS and building equations, respectively. Finally, Table 4 includes a summarization of all the characteristics of the power control optimization, thus the objective function, equalities and inequalities, the objective, the decision variables, dependent variables and parameters, limits and sets.

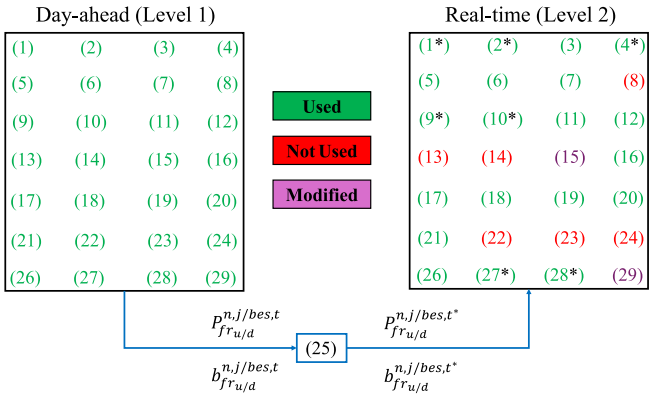

Fig. 3. Integrated equations and transferred variables of power control levels 1 & 2 in Section 5.

Table 2
BESS and EV Parameters of Power Control Model.

Parameters	Explanation	Value
$C^{n,j}_{ev_{pen}}$	EV Charging Penalty	10€/(1%SOC)
$h^{n,j}_{ch}$	EV Charger-Battery Efficiency	0.95
h^{n}_{bes}	BESS efficiency	0.98
$P^{n,j}_{ch_{max}}$	Max EV Charging Power	$\min(P^{n,j}_{ev_r}, 22\ kW)$
$P^{n,j}_{dis_{max}}$	Max EV Discharging Power	$\min(P^{n,j}_{ev_r}, 20\ kW)$
$P^{n,bes}_{ch/dis_{max}}$	Max BESS (dis)charging Power	$0.5C$
$B^{n,bes}_{init}$	BESS Initial Capacity	$0.5B^{n,bes}_{r}$
$B^{n,bes}_{r}$	BESS Rated Capacity	$50\ kWh$
$V^{n,t}$	Instantaneous Node Voltage	230 V
$\Phi^{n,j/bes}$	Number of Used Phases	3
$I^{n,j}_{ch_{max}}$	Max EV Charging Current	$\min(I^{n,j}_{ev_r}, 32A)$
$I^{n,j}_{dis_{max}}$	Max EV Discharging Current	$\min(I^{n,j}_{ev_r}, 29A)$
$S^{n,bes}_{min}$	Min BESS SOC	10%
$S^{n,bes}_{max}$	Max BESS SOC	90%

Table 3
Building Parameters of Power Control Model.

Parameters	Explanation	Value
$C^{n,b}_{hp_{pen}}$	Thermal Discomfort Penalty	10€/(°CΔt)
$C^{n,b}_{pv_{pen}}$	PV curtailment Penalty	10€/(kW Δt)
C_b	Building Thermal Capacity	$4.755\ kWh/K$
V_b	Building Volume	$585\ m^3$
C_{air}	Air Thermal Capacity	$0.279\ Wh/kgK$
ρ_{air}	Air Density	$1.225\ kg/m^3$
$c_{p_{hp}}$	Winter & Summer COP	3.5 & 6
r_b	Building Air Change Rate	$0.3\ h^{-1}$
$T^{n,b}_{min}$	Building Min Temperature	17°
$T^{n,b}_{max}$	Building Max Temperature	27°
$T^{n,b}_{high}$	High Comfort Temperature	23°
$T^{n,b}_{low}$	Low Comfort Temperature	21°
$M1, M2$	Big-M Method Parameters	10
$T^{n,b}_{init}$	Initial Building temperature	22°

6. Data input, case studies & limitations

6.1. Data input & simulation setup

Concerning the simulation setup, the simulations were performed in a Python 3.9 environment, and the MILP model was solved with the Gurobi 11 solver. The timestep of the simulation has been chosen to be 5 minutes for both levels to provide an appropriate trade-off between a reasonably detailed EMS power flow decision-making and computational time. Although a 5-minute timestep is unable to capture transient effects, it is in a position to show the power control behavior concerning PV and BESS utilization, EV charging, HP heating, and participation in the aFRR market. Moreover, the data inputs of the two optimization levels of the power control are listed as follows:

Table 4
Summary of Optimization's features.

Feature	Explanation
Obj. Function	(29)
Inequalities	(4)–(14), (21), (27), (28)
Equalities	(1)–(3), (15)–(20), (22)–(26)
Objective	C_n
Decision Variables	$P^{n,j/bes,t}_{ch/dis}$, $P^{n,j/bes,t}_{fr_u/fr_d}$, $b^{n,j/bes,t}_{ch/dis}$, $b^{n,j/bes,t}_{fr_{u/d}}$, $b^{isp}_{up/down}$, $P^{n,t}_{im}$, $P^{n,t}_{ex}$, $E^{n,j}_{g}$, $P^{n,b,t}_{hp}$, $P^{n,b,t}_{pv_{dev}}$, $T^{n,b,t}_{dev}$
Variables	$I^{n,j/bes,t}_{ch/dis}$, $I^{n,j/bes,t}_{fr_u/fr_d}$, $B^{n,j/bes,t}$, $S^{n,j/bes,t}$, $I^{n,j/bes,t}_{cv_{max,ch}}$, $T^{n,b,t}$, $Q^{n,b,t}_{tot}$, $Q^{n,b,t}_{hp}$, $P^{n,b,t}_{pv_{use}}$
Parameters	$V^{n,t}$, $\Phi^{n,j}$, $B^{n,j/bes}_{init}$, Δt, $h^{n,j}_{ch/bes}$, $T^{n,j}_{a}$, $T^{n,j}_{d}$, $d^{n,j}$, $T^{n,b}_{init}$, C_b, V_b, C_{air}, ρ_{air}, $m^{n,b}$, $I^{n,b,t}_{r}$, U_{sf}, A_{sf}, r_b, T^{i}_{a}, $c^{n,b,t}_{p_{hp}}$, l_{isp}, δ, K, α_{up}, α_{down}, $P^{n,b,t}_{l}$, C^{t}_{buy}, C^{t}_{sell}, $C^{n,b}_{pv_{pen}}$, $C^{n,b}_{hp_{pen}}$, $O^{t,n,b}$, C^{t}_{down}, C^{t}_{up}, $C^{n,j}_{ev_{pen}}$
Limits	$I^{n,j/bes,t}_{r}$, $P^{n,j/bes}_{dis_{max}}$, $P^{n,j/bes}_{ch_{max}}$, $B^{n,j/bes}_{r}$, $P^{n,b,t}_{pv_{max}}$, $T^{n,b}_{high/low}$, G^{n}_{in}, G^{n}_{out}
Sets	T, $[-K, K]$, isp, $\Delta T^{n,j}_{park-da}$, $\Delta T^{n,j}_{park-rt}$

(1) Dutch residential and commercial load consumption probability distribution function (PDF) profiles have been utilized from the Dutch mffbas open database.[1]
(2) With the use of Monte-Carlo Simulation (MCS), 600 EV charger profiles have been developed for home, semi-public, and public chargers (200 per category), utilizing EV driving pattern PDFs (e.g., arrival & departure times, arrival SOCs & requested amounts of energy, etc.) from the Elaad open database.[2]
(3) 200 Winter and Summer PV generation profiles have been developed using MCS with random PV module orientation using weather data (e.g., ambient temperature, incident irradiation, wind speed, etc.) from the Meteonorm database.[3] These weather data have been used for both the PV generation profiles and heating loss calculations to ensure consistency between different LCTs.
(4) The Dutch ENTSO-E platform[4] has been used for the acquisition of energy and reserve price profiles for the day-ahead market (DAM) from three different years (2018, 2019, and 2023).
(5) The LV distribution grid used in the grid-level scenario (see Section 6.2) is based on the work in [56] and was acquired by the Dutch grid operator Enexis Groep.[5]

Finally, the characteristics of the following modules have been used for the considered LCTs:

- HP: a 3 kW-rated Dimplex LIK 8MER reversible HP module.
- PV: a 3 kW-rated HIT N245 PV module.
- EV fleet: The EV fleets for the charger profiles comprise EVs from the following EV pool: "Kona, I3, I-Pace, and Model 3" EVs with a rated power of 11 kW, the "Model X and Model S" EVs of 16 kW, and the "Zoe" EV with 22 kW.
- BESS: The BESS has been developed using Sony US26650FTC1 cells, whose characteristics are derived by the work in [57].

In Fig. 4, daily power profiles for PVs, HPs, and EVs during Winter (upper row) and Summer (lower row) are summarized so that some statistical analysis can be given and supported regarding the input data. Concerning PVs, PV power is generated between [09:00 and 16:00], with

[1] https://www.mffbas.nl/
[2] https://platform.elaad.io/analyses/index.php?url=ElaadNLopendata.php
[3] https://meteonorm.com/
[4] https://transparency.entsoe.eu/
[5] https://www.enexisgroep.com/

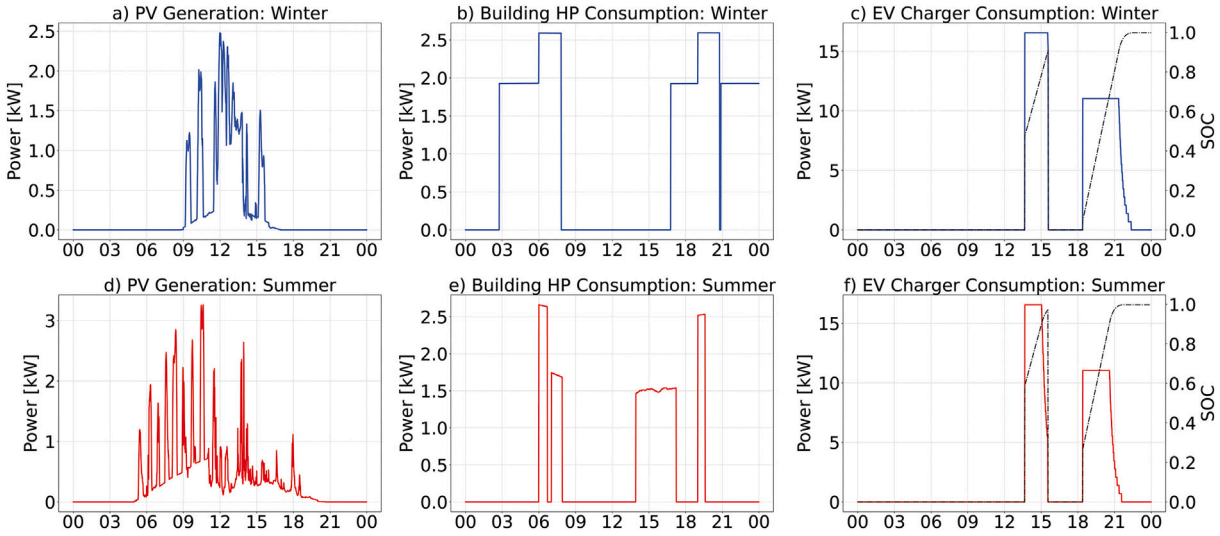

Fig. 4. Daily power profiles for PVs, HPs, and EVs during Winter [a), b), c)] and Summer [d), e), f)].

the highest power peak of 2.5 kW occurring at 12:00. In contrast, PV generation lasts longer during Summer (more specifically between [05:00, 20:00]), having higher power peaks that reach up to 3.2 kW. A weekly average PV rooftop generation is approximately 132 kWh during Winter and 281 kWh during Summer (113% higher). Moreover, regarding the ON-OFF HPs, the high pulses belong to DHW while the low pulses to space heating and cooling in Winter and Summer, respectively. During Winter, building heating is performed with approximately 2 kW HP power, while building cooling requires only 1.5-1.6 kW power due to the more moderate temperature difference with the ambient. Furthermore, building cooling in Summer occurs mostly in the afternoon and endures approximately 4 h, while building heating in Winter occurs at night and in the evening and lasts approximately 8 h (100% longer than cooling). A weekly average HP energy consumption is approximately 286 kWh during Summer and 645 kWh during Winter (126% higher). Finally, there is a 30% higher EV consumption (hence, requested energy) during Winter due to cabin heating, which is visible in Fig. 4(c), since the EVs arrive with a lower SOC than in Fig. 4(f). While the power levels remain unchanged, since the EVs are charged with the rated charging power in uncontrolled charging, the total charging duration can considerably increase (e.g., 30–45' longer).

6.2. Case studies & scenarios

Five case studies are conducted to investigate and compare the individual and cooperative contribution of flexible loads and BESS to energy arbitrage and aFRR provision. Each case study explores a unique aspect of the PCS in order to quantify the capabilities of each asset that is integrated. Constraints are adjusted in each study, treating each aFRR asset as a stand-alone facility. The overall goal is to minimize grid costs, maximize revenues from aFRR provision, while simultaneously minimizing PV curtailment, and ensuring EV owners' and buildings' charging and thermal comfort, respectively. An overview of the LCTs and applications active in each case is given in Table 5, while the case studies are explained as follows:

- Case 1: This baseline case lacks BESS and aFRR services, and comprises only PVs, HPs, EVs, and V2G. This case is derived by [49] and is included to, firstly, show the performance of flexible loads in energy arbitrage, and secondly, serve as validation for this work's PCS and Cases 2–5. It must be noted that V2G denotes the power flow from the EVs to the node, hence the EV discharging for the flexibility of the node and not for aFRR provision to the main grid.

Table 5
Technologies and Applications of each Case Study.

Case	Loads & V2G	BESS	EV: aFRR	BESS: aFRR
Case 1	✓			
Case 2	✓	✓		
Case 3	✓	✓	✓	
Case 4	✓	✓		✓
Case 5	✓	✓	✓	✓

- Case 2: The BESS is added to this case to show the contribution of BESS and its synergy with flexible loads for energy arbitrage. The provision of aFRR reserves by both EVs and BESS is excluded.
- Case 3: In this case, aFRR provision by EVs is added to show the contribution of EVs to power control revenues by ancillary services provision while simultaneously performing energy arbitrage.
- Case 4: In this case, aFRR services are provided only by the BESS to show the contribution of BESS to PCS revenues by ancillary services provision while simultaneously performing energy arbitrage.
- Case 5: Finally, flexible loads and BESS are all included in this case to show their synergy for energy arbitrage and aFRR provision.

It must be noted that, while the authors acknowledge that aFRR is provided by the EVs using the V2G capability, this work distinguishes the terms: V2G and aFRR provision. V2G denotes the discharging of the EVs for the flexibility of the nodes (e.g., building heating, load cover, etc.) and not for the provision of aFRR reserves. This is because the V2G capability is present in all cases, for example, also in the initial Cases 1 and 2, where aFRR reserves are not provided. Hence, to avoid misunderstandings, EV discharging outside of the node for aFRR is explicitly stated as EV aFRR. The five case studies have been investigated for the following three sets of scenarios:

a) Energy and Reserve Price profiles from three different years: 2018, 2020, and 2023. These scenarios aim to investigate the energy and reserve price effect on energy arbitrage and aFRR provision. Grid frequency balance is becoming increasingly important in recent years, and the deviations in energy and reserve prices are more prominent in 2023 than they were in 2018, leading to a higher need for aFRR.

b) One Winter and one Summer day: This set of scenarios is utilized to quantify the seasonal effect and the effect of the weather conditions on the contribution of the different LCTs concerning energy arbitrage (grid power exchange and total power control cost) and aFRR provision (total up- and down-aFRR power delivered and respective PCS revenues).

Table 6
Node characteristics of small grid scenario.

	Node 1 Residential	Node 2 Commercial	Node 3 Mixed
Residential Buildings	5	0	2
Commercial Buildings	0	3	3
Home Chargers	4	2	3
Semi-public Chargers	0	2	0
Public Chargers	0	2	2
BESS (50 kWh)	1	1	1

Table 7
Node characteristics of the large grid scenario.

Nodes	Buildings (PVs, HPs)	Chargers	BESS Capacity [kWh]
1	32	32	320
2	44	44	440
3	18	18	180
4, 5, 6	6	6	60
7, 8, 9, 10	2	2	20
11, 12, 13	1	1	10

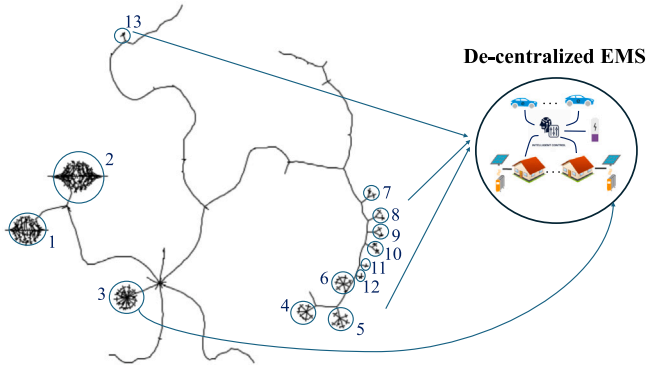

Fig. 5. Distributional EMS of the large grid scenario with the use of aggregators.

These days have been selected randomly from the respective seasons of the three considered years; however, under the following two conditions: firstly, they have energy and reserve prices close to the 3-month average profiles of the respective seasons, as has been done in [58], and secondly, to have notable variations in both price profiles. Finally, these days have been selected as representative of working days of the respective seasons and not weekends, since they constitute the larger part of the month, and are characterized by higher use of commercial buildings and chargers.

c) One small (3-node) grid and one large (13-node) grid scenario to address, firstly, to analyze the influence of the various grid types and the behavior of the occupancy and charging profiles in different buildings and chargers, respectively, on the grid power exchange, delivered aFRR power, and total power control costs and revenues. Secondly, the effect of different grid size levels, especially on aFRR provision, is investigated, providing simultaneous proof of the scalability and expandability of the PCS model to a real grid size level. The specifications of the two grids (buildings, EV chargers, BESS capacities) are summarized in Tables 6 and 7, while Fig. 5 depicts a visual representation of the large grid from Enexis Groep. Finally, $G^{n}_{in/out} = 400\ kW$ & $3.785\ MW$ are the grid power limits for small and large grids, respectively.

6.3. Analysis of selected input LCT profiles

Finally, Fig. 6 depicts in the upper row the pool of PV and EV profiles (for Home and Public chargers) while the respective selected profiles for Nodes 1–3 are depicted in the lower row. As explained, MCS was used to create 90 different PV profiles. In this regard, a tilt angle from 10° to 50° was used with a step of 10° and a module orientation from 0° to 340° with a step of 20°. This was realized for both the Winter and Summer seasons, and then PV profiles were randomly selected for the PV rooftops of Nodes 1–3. As can be observed in the left column of Fig. 6, all nodes' PV profiles fall within the respective generated pool. In a similar manner, MCS was used to create 600 EV charging profiles (200 per category) using different amounts of requested energy and arrival/parking times for Home and (Semi-)Public chargers; arrival SOCs and departure times were adjusted accordingly. This stochastic data was acquired from the Elaad open database, while rated power and current characteristics were used from the pool of EVs. As can be observed in the two right plots of the upper row of Fig. 6, Home charging profiles can be seen mostly after noon when people arrive at home, in contrast with public charging profiles, which are more distributed within the day. Moreover, the higher requested energy (larger profile area) at the home chargers can also be seen here, together with the higher frequency at the public chargers. This is also seen in the randomly selected home and public charging profiles for Nodes 1–3 in the respective plots of the lower row.

7. Results & discussion

This section comprises the results and analysis of the two grid scenarios. Sections 7.1–7.3 are devoted to the small grid scenario concerning power flows, energy, cost, and aFRR provision analysis, respectively, while Section 7.4 comprises the large grid scenario results.

7.1. Power flow analysis

7.1.1. Energy and reserve prices

In Fig. 7, the utilized Winter and Summer energy price profiles (Row 1) with the respective monthly profiles (Row 2) are depicted for 2018, 2020, and 2023. The same has been done in Fig. 8 for the selected and monthly up- and down-aFRR profiles.

Energy and up-aFRR prices are always positive or zero. In this regard, the PCS always pays for buying grid energy and is remunerated for offering up-aFRR reserves. On the contrary, down-aFRR prices can be positive and negative. Negative down-aFRR prices mean that the PCS is remunerated for offering down-aFRR reserves, while it pays the TSO when the prices are positive. Bidding during positive down-aFRR prices has meaning for generators when these prices are lower than their marginal cost; hence, they have cost savings for not producing. Since the aFRR provision assets are BESS and EVs, this is out of the scope of this work, and the PCS is allowed to bid only during negative down-aFRR prices (this can also be seen in (29) where a positive sign is used for down-aFRR reserves bidding). It must be noted that bidding down aFRR at positive prices can, in some situations, be economically attractive for flexible consumption assets. However, this mechanism is not considered in the present work, because limiting down-aFRR participation to negative prices so that aFRR activation does not act as an alternative channel for energy procurement, and charging decisions remain driven by the day-ahead energy schedule rather than by balancing market prices.

As it can be observed, the energy prices are highly increased in 2023, which can reach up to 5.5x times higher during Winter compared to 2018 and 2020. Concerning the aFRR price profiles of the considered days, it can be seen that for all years, especially during Winter, the up-aFRR prices are higher in absolute terms than the negative down-aFRR prices during the largest part of the day. Therefore, the PCS benefits more by providing up-aFRR reserves, hence by decreasing its consumption, especially in recent years 2020 and 2023 due to the abrupt load increase that is supplied by the main grid. Providing down-aFRR reserves, by increasing consumption, is less frequently beneficial, which can be seen by the longer periods of positive and zero down-aFRR prices. On some of the considered days, like Winter 2023, downward imbalance prices never fall below zero, preventing any downward aFRR power delivery. Finally, Fig. 8 shows how the aFRR prices are increased in years 2020 and 2023 compared to 2018, showing a higher need for frequency

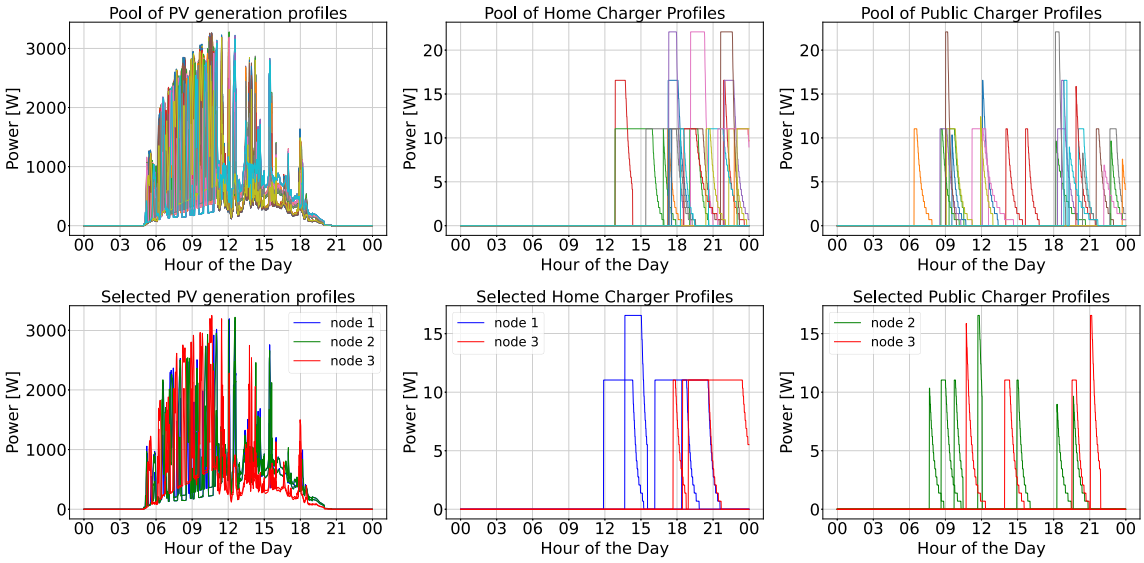

Fig. 6. Pools & selected power profiles of PVs and EVs at nodes 1-3.

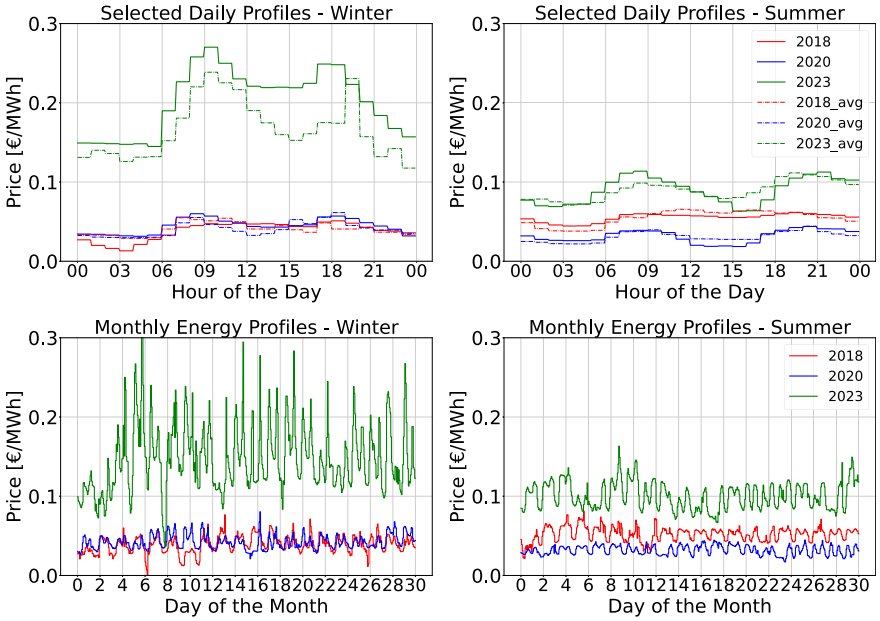

Fig. 7. Winter and Summer energy price profiles: Selected and average (upper row) & Profile Pools (lower row) for years 2018, 2020, 2023.

regulation. This illustrates how aFRR power provision is heavily tied to imbalance price fluctuations.

Regarding the accuracy of the selected energy and reserve profiles in Figs. 7 and 8, it can be seen that the randomly selected profiles for all years and both seasons always fall within the extreme lowest and highest points of their respective profile families. In the upper row of Fig. 7, the average energy profiles for every year and season are also depicted with the selected ones and the standard deviation has been calculated as follows: 0.77%, 0.65%, and 4.13% for Winters 2018, 2020, and 2023, respectively, and 0.56%, 0.51%, and 1.02% for Summers 2018, 2020, and 2023, respectively. As can be seen, all standard deviations are below 5% with the highest deviations observed for the year 2023 due to the higher volatility of the recent energy prices. Due to the extremely high volatility of the aFRR prices in the emerging reserve market, the average up- and down-aFRR profiles (and the respective standard deviations) have not been calculated in Fig. 8; however, it can be seen that both the magnitude and frequency of the up- and down-aFRR calls in the selected profiles agree with the ones in the monthly profiles of each season and year.

7.1.2. Energy arbitrage

Figs. 9 and 10 summarize some power flow examples to provide insights concerning the PCS performance. The synergy of flexible loads and BESS for energy arbitrage without aFRR provision (Case 2) in Node 3 is depicted in Fig. 9 for the Winter and Summer of 2023, together with the daily energy price profiles. Concerning Winter, grid power is imported for building heating, BESS and EV charging mostly during the low energy prices; before 06:00 in the morning and after 20:00 in the evening. Most PV power is exported because it is generated during the high energy prices of [06:00, 15:00]. Additionally, the high energy price period of [17:00, 20:00] is avoided, and grid power is not imported. In contrast, V2G and BESS energy is used instead for base load cover, building

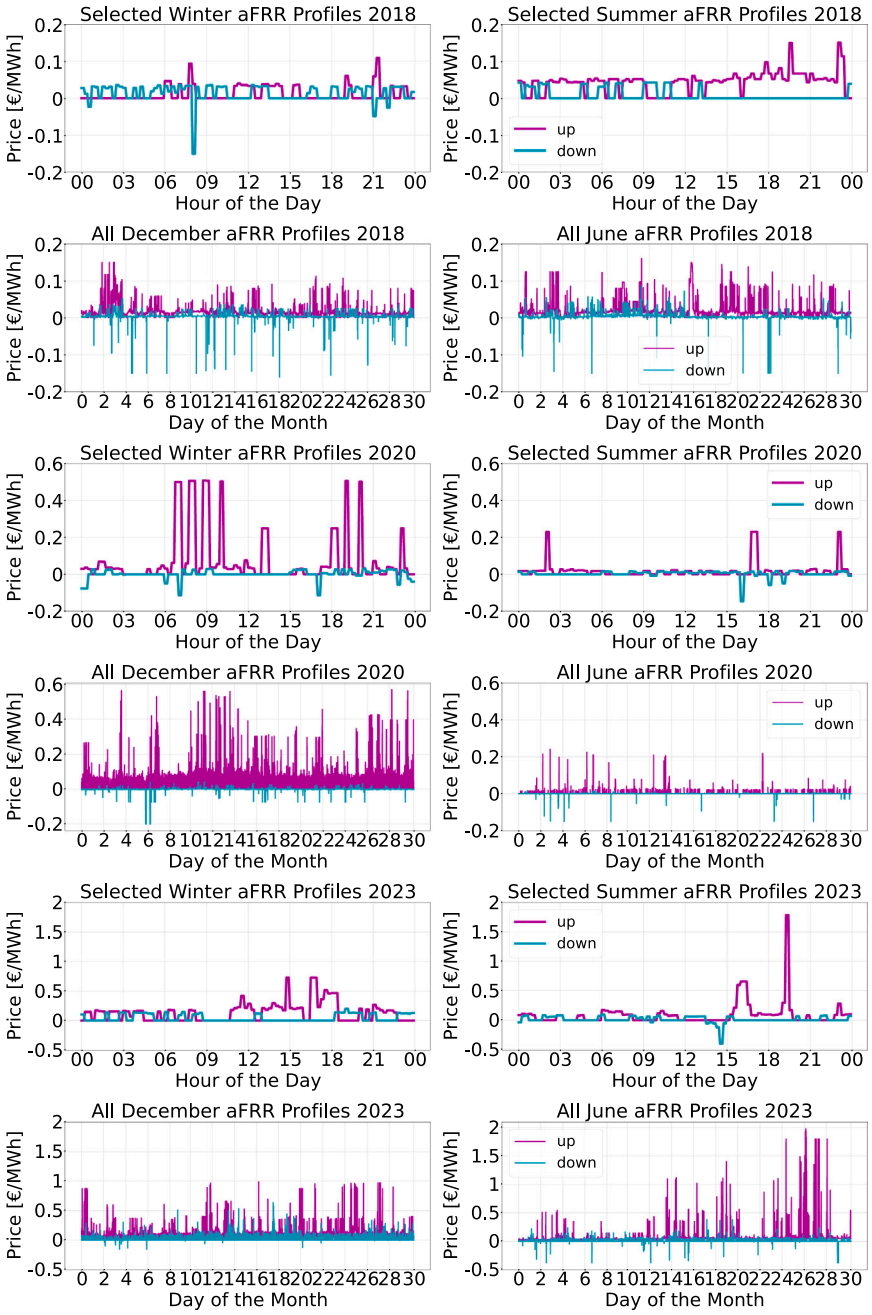

Fig. 8. Winter and Summer energy price profiles: Selected and average (upper row) & Profile Pools (lower row) for years 2018, 2020, 2023.

heating, and EV charging. Concerning Summer, similar observations can be made. For example, the low energy price period of [15:00, 17:00] is utilized for EV and BESS charging, while the BESS is discharged instead of grid power use for EV charging during the energy price peaks of [19:00, 22:00]. Moreover, the PV generation is also exported here for revenues. However, BESS energy is used for the HPs, which are operated here for building cooling during the day [09:00, 16:00]. Furthermore, V2G is less used due to the higher and more prolonged available PV generation, which is preferred due to the round-trip losses of V2G use.

7.1.3. aFRR provision from EVs and BESS individually

The behavior of the power flows of Node 3 during aFRR provision by EVs (Case 3) and the BESS (Case 4) is compared in Fig. 10 for Winter 2023. Taking into account the up- and down-aFRR prices of Winter 2023 in Fig. 8, the high up-aFRR prices of [10:00, 18:00] are greatly taken advantage of in both cases. Additionally, the BESS also exploits the up-aFRR prices of the early morning in Case 4, which cannot occur in Case 3 due to the absence of EVs. Comparing Fig. 10 with Fig. 9, it can be observed that V2G use is highly decreased in Case 3 because EVs are utilized for aFRR reserves provision during the period of [15:00, 18:00]. Instead, the BESS is discharged during this period (e.g., for building heating) and a higher amount of grid energy is imported after 20:00 for EV recharging. On the contrary, regarding Case 4, V2G use is highly increased compared to Case 2 for the flexibility of the node and endures for a longer time period (16:00-20:00), because the BESS is used for aFRR provision. Therefore, it can be seen how the BESS and the EVs are interchangeably utilized for both energy arbitrage and ancillary services provision.

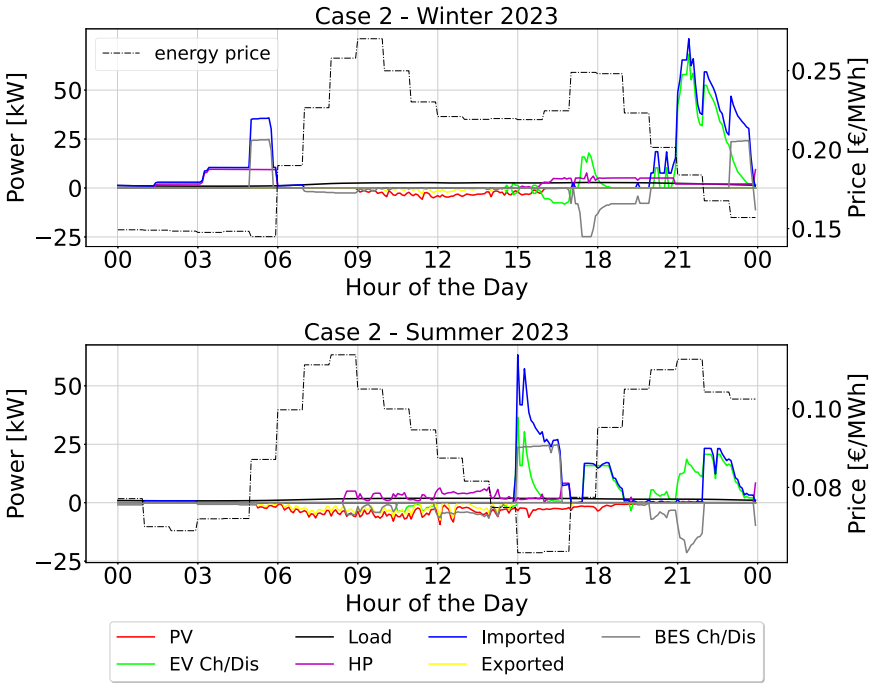

Fig. 9. Energy arbitrage with flexible loads and BESS (Case 2) during Winter and Summer (Node 3 − 2023). Charging/consumption powers are depicted as positive, and discharging/generation powers are depicted as negative.

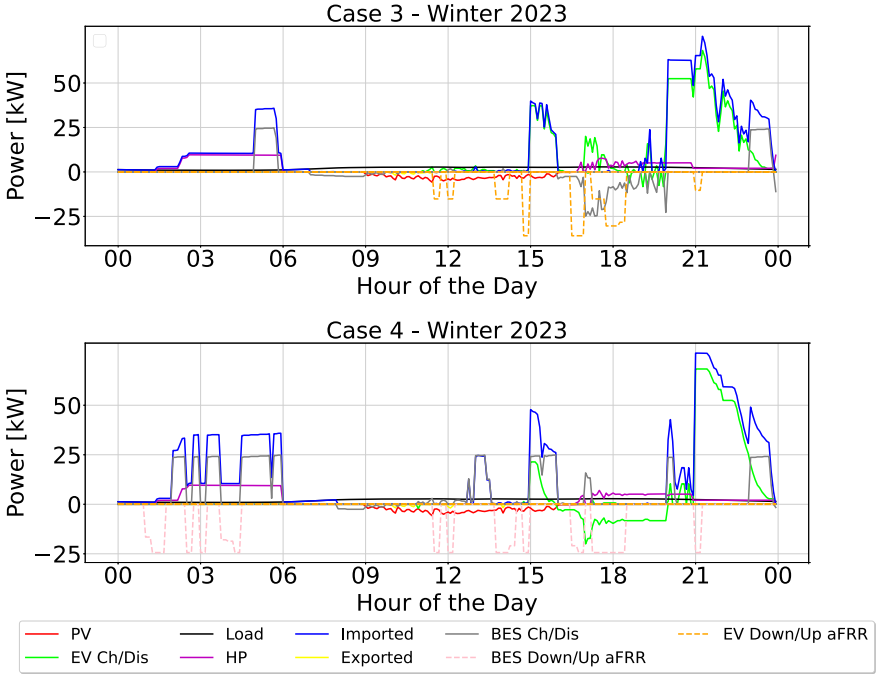

Fig. 10. Energy arbitrage and aFRR provision by flexible loads (Case 3) and BESS (Case 4) during Winter (Node 3 − 2023). Charging/consumption/down-aFRR powers are positive, and discharging/generation/up-aFRR powers are negative.

7.1.4. aFRR provision from EVs and BESS combined

Finally, Fig. 11 depicts the energy arbitrage and aFRR provision by the EVs and the BESS combined (Case 5) for the Winter and Summer of 2023. Fig. 12 is added so that the up- and down-aFRR power flows are isolated for better clarity. Comparing Fig. 11 with Fig. 10, it can be seen that both the EVs and the BESS combine their capabilities to provide up-aFRR simultaneously during the same time periods as before. Moreover, concerning the Summer season, down-aFRR reserves are offered by both assets in the afternoon, exploiting the negative down-aFRR prices at 09:30 and 14:30 (see Fig. 8); consumption increase calls by the TSO are expected during Summer afternoons in recent years due to the high renewable generation (e.g., PVs) that burdens the power grid. On the contrary, no down-aFRR reserves are delivered during Winter 2023 due to the absence of negative down-aFRR prices.

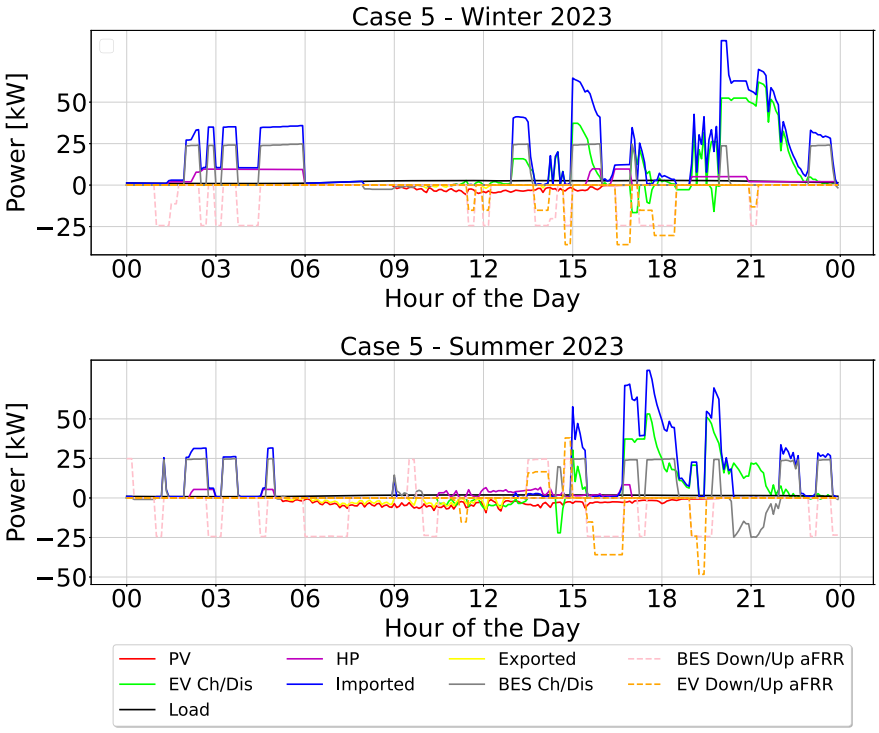

Fig. 11. Energy arbitrage and aFRR provision by both flexible loads and BESS (Case 5) during Winter and Summer (Node 3 −2023). Charging/consumption/down-aFRR powers are positive, and discharging/generation/up-aFRR powers are negative.

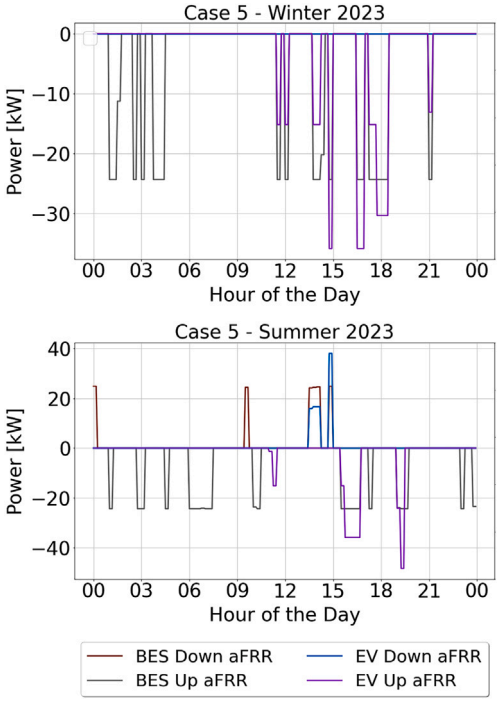

Fig. 12. Isolation of aFRR power flows from EVs and BESS in Fig. 11.

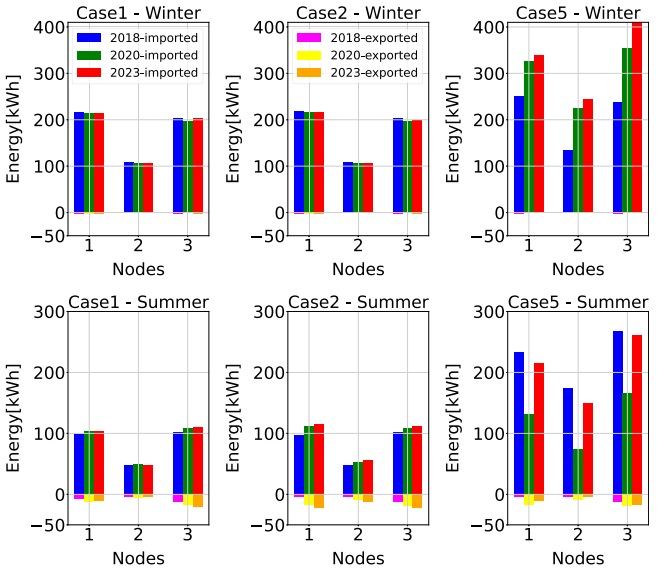

Fig. 13. Imported and exported grid energy comparison during Winter (upper row) and Summer (lower row) for nodes 1–3, years 2018–2023, and Cases 1,2, and 5. Imported powers are depicted on the positive axis, while exported power is depicted on the negative.

7.2. Energy and cost analysis

In this section, the use of grid energy and the total cost of the five investigated cases are compared. In Fig. 13, the imported and exported energy amounts for Cases 1, 2, and 5 during the Winter and Summer of the three years are depicted on the positive and negative axes, respectively. Starting with Case 1, a higher amount of grid energy is imported for all nodes during Winter (approximately 100% increase). This is, firstly, because a 30% higher consumption is needed for EV charging due to cabin heating, and secondly, building heating consumes more energy than building cooling due to the higher temperature difference with the ambient temperature [54]. Moreover, commercial nodes (Node 2) import, on average, 50% lower energy during both Winter and

Summer seasons compared to residential nodes (Node 1) because commercial buildings are less occupied than residential buildings, and EVs arrive with lower SOC at home chargers than at public chargers [56]. Finally, a higher amount of exported energy is seen for all nodes during Summer due to the higher PV generation.

Regarding Case 2 and BESS use, a slight but notable increase in both imported and exported energy can be seen for all nodes during Summer. The use of BESS for the flexibility of the node (EV charging and building cooling) enables higher exportation of PV generation for revenues. Moreover, a higher increase can be seen in years 2020 and 2023 for all nodes due to the higher variation of the energy price profiles (see Fig. 7) which is beneficial for the use of BESS for energy arbitrage and lower power control costs. A similar observation can also be made for Case 1, where the energy arbitrage is performed only by the flexible loads. However, the difference between Cases 1 and 2 remains very low because the loads need the same grid energy amount, and the BESS initial and final SOCs are similar.

Finally, Case 5 is characterized by the highest increase in imported grid energy for all years and nodes. Node 3 is the most affected node, showing a 100% and 150% increase for Winter and Summer, respectively, during 2023. Therefore, as will be seen in the next section it is the node that provides the highest amount of aFRR reserves due to its highest flexibility since it comprises both residential-commercial buildings and home-public chargers. Moreover, concerning the comparison between the different years, 2023 is characterized by the highest increase in grid energy; hence, the highest provision of aFRR reserves due to the higher reserve prices and duration of need for aFRR reserves (Fig. 8). For the same reason, 2020 is more beneficial than 2018 for the Winter season, while the opposite applies for Summer.

Figs. 14 and 15 summarize the cost analysis of this work and also serve as validation of this work's Cases 2–5 compared to Case 1, which is based on [49]. Fig. 14 shows in the first row the total cost for Nodes 1–3, Cases 1–5, during Winter and Summer 2023. The total cost is equal to the energy arbitrage (EA) cost minus the aFRR revenues, which are depicted in the plots of the second row below. While a slight decrease is seen from Case 1 to Case 2, the highest cost decrease is shown for the aFRR provision cases, especially for Case 5, which exploits both assets (EVs and the BESS), and for Node 3. Especially for the Summer season, the costs for all nodes result in negative numbers ($-60e$ for Node 3 in Case 5), which means that the PCS is actually remunerated and not charged for the power control operation. Furthermore, as already explained, the ancillary services provision is mostly beneficial for Node 3 due to its highest flexibility because of the variety of EV fleets. Node 3 (mixed node) is characterized by longer connection times and more simultaneously connected EVs. The number of connected EVs directly influences their ability to participate in the aFRR market, as it determines the available battery storage capacity and aFRR power potential. For the same reason, Node 3 is the only node that has the highest cost decrease during both seasons in Case 3 (aFRR provision by EVs) compared to Case 4 (aFRR provision by the BESS), since the BESSs are all 50 kWh-rated for all three nodes. Finally, the increase in aFRR revenues but also in the EA cost, which is justified since a higher grid energy amount is imported, can be seen in the second row of Fig. 14.

To strengthen our observations about the total cost of the investigated cases, Fig. 15 summarizes the cost reduction achieved in Cases 2–5 compared to Case 1 (power control only with flexible loads) for Winter (first row) and Summer (second row) for all the investigated nodes and years. It can be seen that Case 5 always offers the highest cost reduction, which is almost always above 40% in 2018, and 100% in the recent years 2020 and 2023, while it reaches up to 900% and 800% for Node 2 during Winter 2020 and Summer 2023, respectively. On the contrary, Case 2 (the use of BESS without aFRR provision) offers, in most nodes and scenarios, the least cost reduction. Furthermore, the use of BESS for aFRR provision (Case 4) is more beneficial than the use of EVs (Case 3) except for some scenarios for Node 3, such as Winter and Summer 2023. This is expected because the BESS is present and is capable of offering

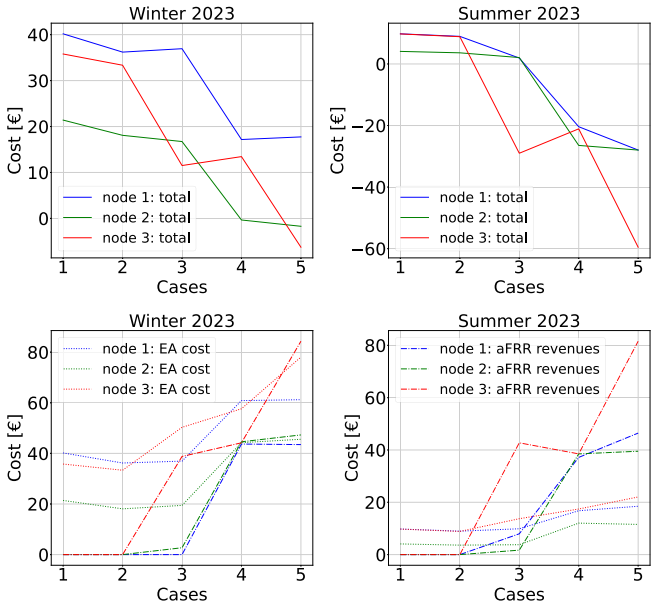

Fig. 14. Energy arbitrage (EA) cost, aFRR revenues, and total cost comparison for nodes 1–3, Cases 1–5, Winter & Summer 2023, where $total = EA - aFRR$. Validation against Case 1 of [49].

reserves during the whole simulation period, in contrast with the EV fleets. Moreover, Node 2 shows the highest cost reduction for all cases and scenarios, which is justified by the fact that the PCS cost of Node 2 is already the least compared to the other two nodes in Case 1; hence, the additional aFRR revenues are most significant compared to the already EA cost.

Finally, it can be seen that in recent years, the potential of cost reduction by offering ancillary services is further increasing. For example, the cost reduction in Summer 2020 and Summer 2023 reaches up to 4x and 8x times compared to Summer 2018. The only exception constitutes the transition from Winter 2020 to Winter 2023 because the aFRR price levels of the two years are comparable, while the energy price levels of 2023 reach up to 4.5x times higher than the respective levels of 2020. Hence, Case 1 of Winter 2023 is characterized by a much higher cost than Case 1 of Winter 2020. However, while it might seem that the cost reduction due to ancillary services provision is lower during the Winters of recent years, according to the author's opinion, it is evident that the participation of the PCSs in such services is becoming increasingly important due to the much higher energy prices.

7.3. aFRR provision analysis

In this section, the provided energy for up- and down-aFRR reserves for the investigated cases and scenarios is summarized to strengthen the insights of the previous sections. Fig. 16 depicts the respective results for all nodes during Winter and Summer 2023. The up-aFRR reserves are depicted on the positive y-axis, while the down-aFRR reserves are on the negative side. The first main observation is that the provided up-aFRR reserves are vastly higher than the respective down reserves and can reach up to 400% higher (200 kWh compared to 50 kWh: Node 3 - Summer 2023). As seen in Fig. 8, especially during the considered Winter days, only up reserves are provided, due to the beneficial up-aFRR price profiles, while there is a lack of negative down-aFRR prices for downward aFRR capacity scheduling. This is expected in Winter, when the TSO most often needs up-regulation due to the high load consumption. Furthermore, as explained before, the BESS provides more up- and down-aFRR energy than the EVs since it is always present, while EVs arrive and depart following specific patterns and must maintain a minimum departure state of charge to ensure user comfort. For example,

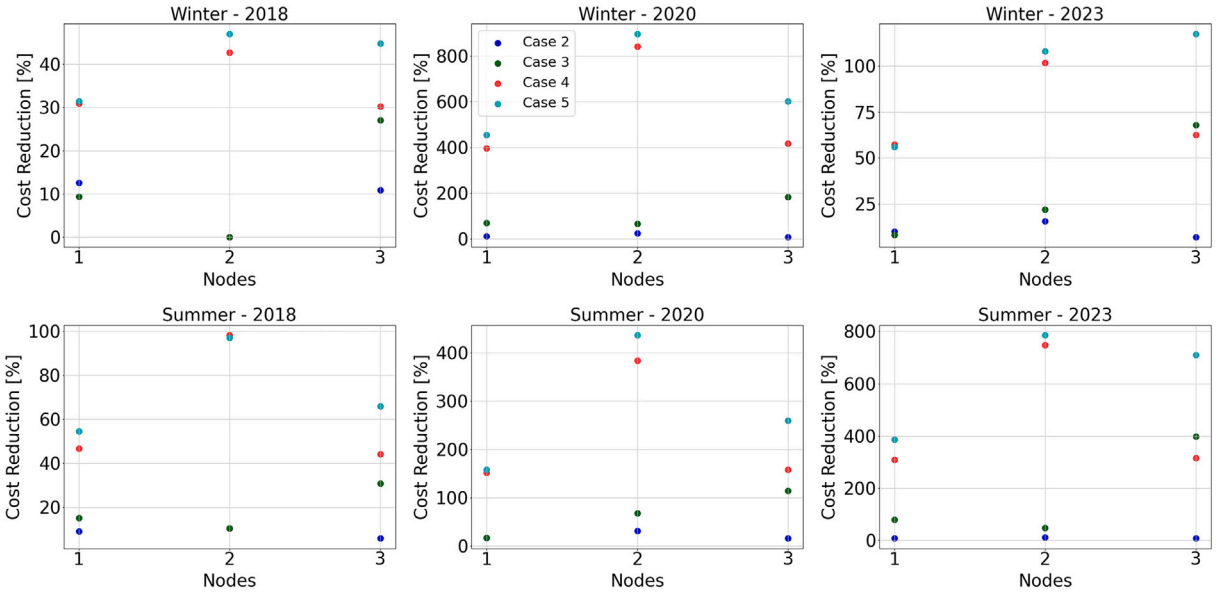

Fig. 15. Summary of cost reduction by BESS utilization and aFRR provision during Winter (upper row) and Summer (lower row) for nodes 1–3, years 2018–2023, and Cases 2–5: Validation against Case 1 of [49].

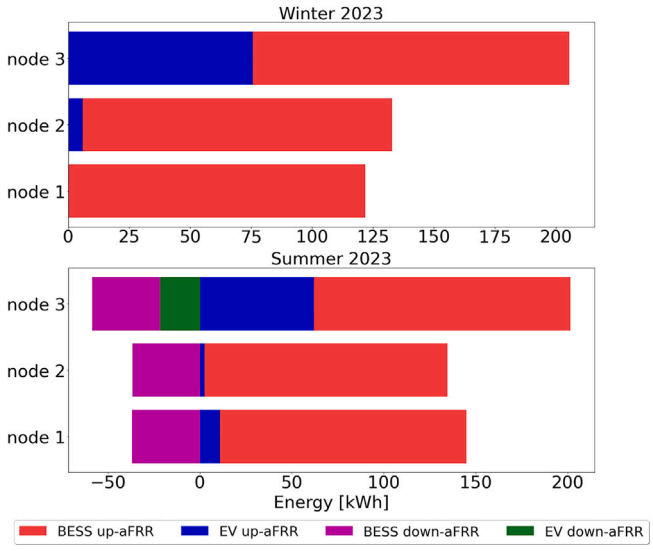

Fig. 16. Upward and downward aFRR provision by EVs and BESS during Winter and Summer: Nodes 1–3, Case 5, 2023.

40 kWh and 140 kWh of down and up reserves are provided by the BESS compared to 25 kWh and 60 kWh by EVs in Node 3 during Summer 2023. It is also noticed that the BESS provides the same aFRR energy at all nodes during each season, which is rational since all BESSs are 50kWh-rated and start and end with the same SOC (50% considered in this work). Finally, it can also be seen here that Node 3 has the capability of providing the highest amount of up- and down-aFRR energy by EVs due to its variety of EV fleets; 60 kWh of up-aFRR energy compared to 5 kWh and 12 kWh of Nodes 2 and 1, respectively, during Summer.

Fig. 17 summarizes all up- (first row) and down-aFRR reserves (second row) provision for all nodes, cases, seasons, and years, where W and S denote Winter and Summer, respectively. The highest provided upward and downward aFRR capacities are 200 kWh and 60 kWh, respectively, for Node 3 in the year 2023. Regarding upward capacity, Cases 4 and 5 provide the highest aFRR amount, especially during the Winters of 2020 and 2023, while Node 3 consistently provides more capacity than the other two nodes for all years and cases. Moreover, comparing the seasons, while more up-regulation was delivered during Winter than Summer in 2020 (expected due to the high grid load consumption in Winter), a high increase can also be seen during Summer in 2023. Finally, comparing the years, the higher need, and hence, higher potential for participation of the PCS in the imbalance market is evident in recent years.

Regarding downward capacity, the superiority of Cases 4 and 5, and Node 3 can also be seen here. Moreover, observing the Winter cases of the years 2018-2023, the scheduling and provision of downward aFRR capacity keep decreasing as the year increases. On the contrary, an increasing trend can be seen during the Summer throughout the years. This is also expected due to the general grid load consumption increase during Winter and RES generation during Summer; hence, the TSO needs less downward regulation during Winter and more during Summer in recent years. However, the downward amount compared to the upward amount remains considerably lower. This is because, firstly, the TSO needs increasingly more upward regulation during the Winter (both in magnitude and duration). Secondly, as explained, upward regulation can also increase during Summer in the most recent years, such as 2023, in different time periods than the downward, due to the use of LCTs, e.g., EV charging during the evening. All of these trends can also be seen in Fig. 8. However, it must be noted that since the simulations of this work are daily, the insights regarding the comparison of the seasons should not be generalized unless a seasonal analysis is performed.

Finally, Table 8 summarizes all main energy and economic results (e.g., imported/exported energy, EV/HP consumption, up- and down-aFRR provided energy, energy cost, and aFRR revenues, etc.) of Node 3 for Cases 2–5 of years 2018 and 2023 for a clearer view of the power control performance.

7.4. Large grid scenario results

The grid-level example is simulated for Cases 1, 2, 4, and 5; however, only for the Winter and Summer seasons of 2023, due to long computational times (> 12 hours). The simulations show consistent results compared to the small grid example regarding the cost savings and the related synergy of the LCTs acting as aFRR provision assets. Table 9 shows the total grid costs summed over all nodes for the Winter season.

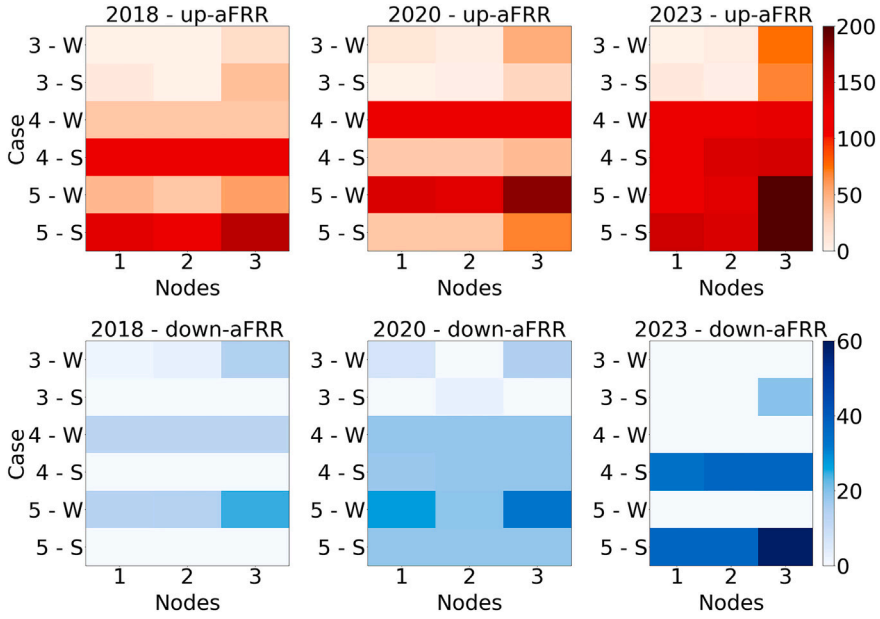

Fig. 17. Summary of upward (upper row) and downward (lower row) provided aFRR energy (kWh) during Winter (W) and Summer (S), Nodes: 1-3, Cases 3-5, Years: 2018, 2020, 2023.

Table 8
Summary of main energy and economic results for Node 3 of the small grid scenario.

	Case 2				Case 3				Case 4				Case 5			
	2018		2023		2018		2023		2018		2023		2018		2023	
Metrics	Win	Sum	Win	Sum	Win	Sum	Win	Sum	Win	Sum	Win	Sum	Win	Sum	Win	Sum
Imported Energy (kWh)	202.9	101.8	199.7	112.6	211.3	148.6	279.8	168.9	228.3	228.4	332.4	217.3	239.2	268	416.1	261.2
Exported Energy (kWh)	4.1	12.2	4	22.7	4.1	12.3	0.9	22.1	4.2	12.3	1.2	19	4.1	12.2	1.2	16.9
EV Load (kWh)	100.3	72.5	108.7	76.7	112	116.3	181.9	127.6	110.3	72.6	131.3	97.7	112.1	110.2	188.5	131.1
HP Load (kWh)	64.4	28.4	60.9	27.7	65	28.3	63	27.3	63.7	27.7	62.2	27.3	64.3	27.7	62.7	27.4
Up-aFRR Energy (kWh)	0	0	0	0	20.4	41.4	74.5	68.5	36.5	122.3	127.4	139.9	57	158.1	205.5	201.5
Down-aFRR Energy (kWh)	0	0	0	0	14.5	0	0	19.3	12.2	0	0	36.8	24.7	0	0	58.5
V2G Energy (kWh)	0.8	0	8.9	4.3	4.7	0	3.7	1.3	10.9	0	31.6	25.1	2.5	0.5	9.1	14
Energy Cost (€)	6.1	4.7	32.5	6.7	6.7	7.5	50.1	11.6	7.1	11.7	57.4	15.6	7.8	14.1	77.8	20.4
aFRR Revenue (€)	0	0	0	0	1.7	4.2	38.8	42.7	2.4	9.2	44.2	38.5	4.1	12.9	84.3	81.6
Total Cost (€)	6.1	4.7	32.5	6.7	5	3.3	11.3	−31.1	4.7	2.5	13.2	−22.9	3.7	1.2	−6.5	−61.2

Table 9
Cost and cost reduction of Cases 2, 4, and 5 compared to Case 1 for the large grid scenario.

Case	Total Grid Cost (*e*)	Percentage Difference
Case 1	€ 213.52	–
Case 2	€ 201.65	−5.56%
Case 4	-€ 38.32	−117.95%
Case 5	-€ 890.33	−516.98%

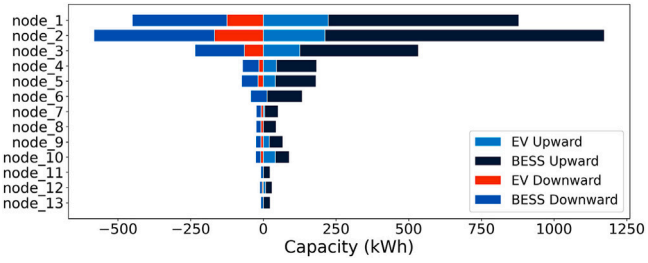

Fig. 18. Total BESS and EV up- and down-aFRR provided energy for nodes 1–13 for Case 5.

Similar to the small grid scenario results, Case 4 is the first case to show high profits (118% savings) compared to Case 1 due to revenue generated by aFRR participation. In addition, Case 5 shows the highest savings (517%) due to the presence of both EVs and BESS to participate in the aFRR market. The respective cost savings of Cases 4 and 5 in the small grid scenario are 810% and 900%, respectively. While the cost savings (in percentage) of the large grid scenario for Cases 4 and 5 are lower than the respective savings of the small grid scenario due to the larger size of the grid (a larger grid already has a much higher power control cost from Case 1), the importance of the synergy of the EVs and the BESS for aFRR provision in a PCS is also shown here in this grid scenario.

Fig. 18 illustrates consistent scaling between aFRR provision and node size (node size decreases with numbering), where downward energy is again indicated in the negative direction. Similar to the small grid scenario simulation, more upward than downward power is delivered due to the already explained higher potential; 1150 kWh up-aFRR provided energy compared to 600 kWh down-aFRR energy for Node 2. Moreover, it can be seen that the size of the node has a considerable effect on both the magnitude of aFRR provision by EVs and the BESS

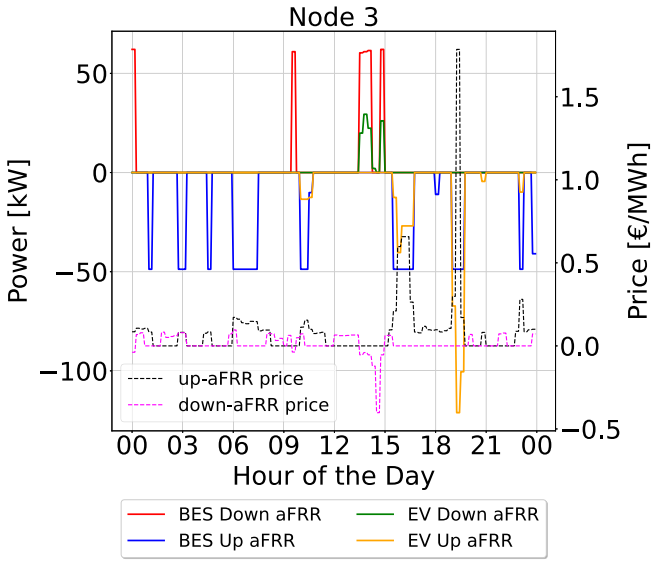

Fig. 19. BESS and EV up- and down-aFRR powers for Node 3 of large grid scenario in Case 5.

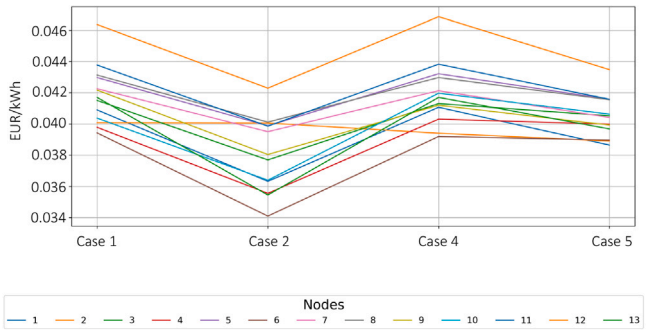

Fig. 20. Average energy arbitrage cost per imported grid kWh for Cases 1, 2, 4, and 5 in the large grid scenario nodes.

individually, as expected, but also concerning the comparison between them. For example, EVs provide negligible aFRR energy at the very small Nodes 11–13. However, the up- and down-aFRR provided energy by EVs already constitute 19% of the respective energy amounts provided by the BESS for the average-size Node 5. Additionally, the percentage is even higher for the large nodes, such as Node 1 and Node 3; for example, the provided down-aFRR energy by EVs constitutes 28.6% of the energy provided by the BESS (100 kWh compared to 350 kWh) while the respective percentage for up-aFRR reserves is 38.5% (250 kWh compared to 650 kWh). Hence, it is proven that in larger nodes (or grids) that comprise a vast number of loads, the contribution of loads to ancillary services provision increases and can become comparable to a stationary BESS, even if the BESS capacity increases. In Fig. 19, the up- and down-aFRR powers for the BESS and EVs at Node 3 of the large grid scenario are depicted for Case 5 together with the respective reserve price profiles to show the timeline of the provided ancillary services by the two assets.

In Fig. 20, we see a similar pattern for all nodes in the average cost of imported energy (total energy arbitrage cost per imported grid energy in e/kWh as in the small grid scenario results (Fig. 14). Case 2 exhibits the lowest imported energy cost since the addition of the BESS increases the flexibility of every node compared to Case 1 to perform energy arbitrage for higher revenues, exploiting the low and high energy price peaks of the energy price profiles. In contrast, incorporating aFRR provision in Cases 4 and 5 results in a significant increase in the average cost of imported energy compared to Case 1. This rise is due to the BESS charging at higher day-ahead prices, to subsequently discharge as upward aFRR power or the opposite for the provision of the downward aFRR power. Therefore, these additional costs are compensated by the revenue generated from providing aFRR services, as it was seen for the small grid scenario in Fig. 14.

Finally, Table 10 summarizes all main energy and economic results (e.g., imported/exported energy, EV/HP consumption, up- and down-aFRR provided energy, energy cost, and aFRR revenues, etc.) of 4 representative nodes: Nodes 1 and 3 for the large-scale, Node 5 for the medium-scale and Node 12 for the small-scale nodes.

8. Discussion

8.1. Summary of findings

Taking everything into consideration, this work compared the individual and combined contribution of flexible loads and BESS to energy arbitrage and aFRR provision. This has been conducted in a PCS handled by aggregators of the aforementioned assets formulating an optimization of the aggregators' point of view and accounting for various influencing factors, such as different seasons, energy and reserve price profiles, grid types, and sizes. The most important findings of the work can be summarized as follows:

1) BESS are generally capable of offering and providing more upward and downward aFRR reserves than EVs due to the lower connection time, EV driving patterns uncertainty, and requested charging energy. However, it was shown that in larger grids or larger nodes that comprise a higher amount of EV chargers and incoming EV fleets, the provided upward and downward reserve amounts are highly increased and can become comparable to the respective amounts provided by the BESS. For example, while BESS provided x12 and x5 higher up- and down-aFRR reserves, respectively, compared to EVs in the small grid, the contribution of EVs reached up to 28.6% and 38.5% for up- and down-aFRR reserves in the large grid.

2) As expected, the greatest earnings are achieved when both BESS and EVs participate in energy arbitrage and aFRR provision reaching up to $-60e$ compared to $+10e$ of energy arbitrage at Node 3. The inverse sign means that the PCS of the node was actually remunerated when it was allowed to provide ancillary services with both assets. This is justified not only by the fact that both assets participate in the imbalance market and provide regulation reserves, but also because one asset (e.g., EVs) can take responsibility for energy arbitrage, such as building heating during low energy prices, while the other (e.g., the BESS) provides aFRR reserves to the TSO, and vice versa.

3) Mixed nodes that integrate both residential-commercial buildings and home-public chargers are consistently capable of delivering the majority of aFRR energy while simultaneously performing energy arbitrage. For example, Node 3 provided up to 200 kWh upward and 60 kWh downward compared to the respective 150 kWh and 40 kWh values of Node 1. Moreover, it was the only node that provided notable aFRR reserves from the EVs. This is because of their higher flexibility due to the variety of flexible loads, such as those of the incoming EV fleets, resulting in a higher duration of EV connectivity during the day, more simultaneously connected EVs, etc.

4) V2G, hence EV discharging for the node flexibilities such as building heating or load cover, is less utilized when there is available PV generation (e.g., Summer season) or a BESS due to higher round-trip power losses that usually overcome the earnings from energy arbitrage. Hence, V2G use is left for activities only in extreme cases, such as building heating during energy price peaks when no PV generation is available [49]. However, when a PCS enables reserve market participation in its power control, the use of V2G for energy arbitrage is less dependent on seasonal effects or the presence of other assets. For example, V2G might be used for the flexibility of the nodes when the BESS is used for aFRR provision, since the power losses are compensated by the additional earnings. Thus, when the PCS participates in ancillary services, the use of V2G for the rest of the node

Table 10
Summary of main energy and economic results for nodes 1, 3, 5, and 12 of the large grid scenario.

	Node 1			Node 3			Node 5			Node 12		
Metrics	Case 2	Case 4	Case 5	Case 2	Case 4	Case 5	Case 2	Case 4	Case 5	Case 2	Case 4	Case 5
Imported Energy (kWh)	629.3	712	851.5	554.8	640.6	705.2	163.5	252.8	282.6	20.6	117.4	109.6
Exported Energy (kWh)	146.6	142.1	129	75.7	67.9	65.5	31.3	21.3	18	5.5	3.2	3.2
EV Load (kWh)	581.8	547	664	446.4	455	499.2	120.9	121	151.9	14.2	14.2	18.1
HP Load (kWh)	163.7	164.1	164.4	92.2	91.4	92.4	30.5	30.8	30.8	5.3	5.2	5.2
Up-aFRR Energy (kWh)	0	437.6	854	0	329.4	583.4	0	133.7	163	0	33.2	45.4
Down-aFRR Energy (kWh)	0	236.9	456.8	0	136.8	238.4	0	76.8	76.8	0	8.8	12.8
Energy Cost (€)	41.2	48.5	66.3	43	51.6	59.4	11.1	20	23.5	0.8	8.9	8.5
aFRR Revenue (€)	0	38.3	176.1	0	37	99.6	0	38	58.6	0	38	42.7
Total Cost (€)	41.2	10.2	−109.8	43	14.6	−40.2	11.1	−18	−35.1	0.8	−29.1	−34.2

services (e.g., load cover) can vastly increase because the earnings from the ancillary services compensate for the high round-trip power losses.

5) Upward aFRR reserves are increasingly needed for the power grid in recent years, especially during Winter, reaching up to 200 kWh daily in 2023 compared to the maximum of 120 kWh in 2018, and PCSs that can integrate participation in the imbalance market can be greatly contributive and achieve high cost savings. On the contrary, downward aFRR reserves are less needed than upward, possibly due to the higher use of LCTs. Nevertheless, a notable increase is seen during the Summer of recent years. For example, while a maximum of 30 kWh delivered downward reserves was observed in 2018, it reached up to 60 kWh for the Summer of 2023. However, it must be noted again that this insight is highly dependent on the daily volatility of energy and reserve prices and their interrelations. A seasonal analysis should be performed to strengthen this point.

6) Overall, summarizing the investigated influencing factors, the grid type and the seasonal effect were found to be the most important factors since they highly affect both energy arbitrage and ancillary services provision. Energy and reserve prices follow since they had a strong effect on the amount of provided ancillary services; however, they were less significant regarding energy arbitrage. Finally, the grid size is characterized as the least important influencing factor since most of the work's insights remained similar in the two grid scenarios.

8.2. Limitations

Firstly, while some uncertainty has been considered between the two levels for buildings' occupancy and EV driving patterns, a lot of uncertainty sources (building types, LCTA modules, price uncertainty, etc.) have been neglected. For example, the study uses DA prices for power optimization and assumes perfect imbalance price forecasts, missing real-time price dynamics. Moreover, the maximum EV arrival and departure time uncertainties have been set at 15', as, firstly, has also been considered in previous studies, and secondly, because of the assumption that the EV drivers are aware of the importance of delays when they participate in grid ancillary services. However, the authors recognize that this assumption is optimistic and constitutes an important limitation of this study, and more extended delays, reaching up to 1h, should be investigated in further scenarios.

Secondly, it has been assumed that the aFRR bid is always accepted as a whole in the reserve market and called for deployment in real-time due to the zero-bid of RES-integrated balance responsible parties. Real-world scenarios involve partial activations and a minimum bid size of 1 MW.

Thirdly, the HP COPs are considered constant and equal to the average 3.5 and 6 for Winter and Summer, respectively; however, notable fluctuations can be induced due to changing weather conditions, such as ambient temperature. Additionally, all LCT ramping rates are considered instantaneous due to the 5' simulation step.

Moreover, this work has investigated only daily simulations during Winter and Summer due to the high computational time. While the days have been selected to have price profiles close to the 3-month average seasonal profiles, and the weather data has been derived from the Meteonorm database, which averages them for the past 10 years, daily simulations can be prone to accuracy errors due to the uncertainty of energy and reserve price profiles. Additionally, the considered days have been selected to be working days due to the higher use of commercial buildings and chargers; thus, the use of weekends could have a significant impact on this work's results.

In this work, electricity consumption and injection are priced using hourly day-ahead wholesale electricity prices only. Network tariffs, taxes, levies, and other retail charges are not included. As a result, the reported cost outcomes represent marginal wholesale energy costs rather than final prosumer electricity bills, which may affect absolute profitability levels.

The model represents the dynamic nature of aFRR through activation uncertainty but does not explicitly model hourly system reserve requirements or market-clearing selection/competition. As a result, volume procurement effects are not captured. Moreover, down aFRR participation by electric vehicles and battery energy storage systems is restricted to negative prices. As a result, potential use of positive priced down aFRR as an alternative charging or energy procurement mechanism is not considered, which may reduce down aFRR volumes and affect the reported cost outcomes.

Finally, battery degradation has not been incorporated in this work, which highly affects cost reduction and revenue, especially in studies of ancillary services provision due to the high frequency of battery charging and discharging.

9. Conclusions

This work has enhanced the bi-level multi-objective PCS of PVs, EVs, HPs, and BESSs, which formulated from the perspective of aggregators, focuses on energy arbitrage, participation in the aFRR market while simultaneously respecting the grid limits, the charging and thermal comfort of the customers, and maximizing PV self-consumption. The contribution of the flexible loads and the BESS to the energy arbitrage and aFRR reserves provision has been compared under multiple influencing factors, such as different seasons, grid types and sizes, and energy/reserve prices. The findings demonstrate that the participation of the PCS in the reserve market provides consistently higher than 100% cost reduction in recent years, reaching up to 900% compared to power control only for energy arbitrage. Moreover, these numbers can be achieved more effectively when more than one asset provides ancillary services (e.g., EVs and BESS), not only because they can both actively participate in the provision of the services, but also because they can share the other responsibilities. While the always-present BESS is able to contribute more to ancillary services provision compared to the uncertain nature of the EV fleets, the contribution of EVs increases to a notable 38.5% compared to the BESS at grids or nodes of larger size. Finally, mixed nodes that comprise both residential-commercial buildings and home-public chargers have a higher potential in bidding and providing up- and down-aFRR reserves due to higher flexibility. Results

demonstrate a 5x and 12x higher potential of mixed nodes compared to residential and commercial nodes, respectively.

Regarding future work, the consideration of more uncertainties that are present in PCSs is recommended for the DA level and their management on the RT level. Moreover, the use of weekly and seasonal simulations is strongly recommended since it would strengthen the insights concerning the season comparison and also show intra-weekly effects. Furthermore, the probability of no acceptance and partial deployment is proposed to further address the uncertainty of the reserve market. Additionally, accounting for variable HP COPs is recommended to encapsulate the weather effect on the PCS results, especially concerning the building heating. Finally, the integration of a battery degradation model is proposed to economically evaluate the battery usage for ancillary services provision.

CRediT authorship contribution statement

Sam Warmerdam: Writing – original draft, Software, Methodology, Investigation, Data curation. **Nikolaos Damianakis:** Writing – review & editing, Writing – original draft, Validation, Software, Data curation, Conceptualization. **Gautham Ram Chandra-Mouli:** Writing – review & editing, Supervision, Resources, Project administration, Funding acquisition.

Declaration of competing interest

The authors declare the following financial interests/personal relationships which may be considered as potential competing interests:

Nikolaos Damianakis reports that financial support was provided by Dutch Research Council. If there are other authors, they declare that they have no known competing financial interests or personal relationships that could have appeared to influence the work reported in this paper.

Acknowledgments

This study is funded by the Dutch Research Council (NWO) as part of the ongoing research project NEON with project number 17628 of the research program Crossover. Moreover, I would like to personally thank Enexis Groep for the acquisition of the used distribution grid.

Data availability

Data will be made available on request.

References

[1] European Commission, REPowerEU: affordable, secure and sustainable energy for Europe, 2023. [Online]. Available: https://commission.europa.eu/strategy-and-policy/priorities-2019-2024/european-green-deal/repowereu-affordable-secure-and-sustainable-energy-europe_en (accessed: 22 April 2023).

[2] Netbeheer Nederland, Wachtlijsten voor Stroomaansluitingen Nemen Toe, May 2023. [Online]. Available: https://www.netbeheernederland.nl/artikelen/nieuws/wachtlijsten-voor-stroomaansluitingen-nemen-toe (accessed: 22 April 2024).

[3] Rijksdienst voor Ondernemend Nederland (RVO), Cijfers over elektrisch rijden in Nederland, 2023. [Online]. Available: https://www.rvo.nl/onderwerpen/duurzaam-ondernemen/energie-en-milieu-innovaties/elektrisch-rijden/stand-van-zaken/cijfers.

[4] N. Damianakis, G.R.C. Mouli, P. Bauer, Grid impact of photovoltaics, electric vehicles and heat pumps on distribution grids — an overview, Appl. Energy 380 (2025) 125000.

[5] M. Rüdisüli, S.L. Teske, U. Elber, Impacts of an increased substitution of fossil energy carriers with electricity-based technologies on the Swiss electricity system, Energies 12 (12) (May 2019) 2399. https://doi.org/10.3390/en12122399

[6] B. Asare-Bediako, W.L. Kling, P.F. Ribeiro, Future residential load profiles: scenario-based analysis of high penetration of heavy loads and distributed generation, Energy Build. 75 (2014) 228–238.

[7] R. Gupta, A. Pena-Bello, K.N. Streicher, C. Roduner, Y. Farhat, D. Thöni, M.K. Patel, D. Parra, Spatial analysis of distribution grid capacity and costs to enable massive deployment of PV, electric mobility and electric heating, Appl. Energy 287 (2021) 116504.

[8] Netbeheer Nederland, Wachtlijsten nemen toe, Feb 2024. [Online]. Available: https://www.netbeheernederland.nl/artikelen/nieuws/wachtlijsten-nemen-toe (accessed: 22 April 2024).

[9] B. Thormann, T. Kienberger, Evaluation of grid capacities for integrating future e-mobility and heat pumps into low-voltage grids, Energies 13 (Sep 2020) 5083.

[10] A. Navarro-Espinosa, L.F. Ochoa, Probabilistic impact assessment of low carbon technologies in LV distribution systems, IEEE Trans. Power Syst. 31 (3) (2016) 2192–2203.

[11] J.-T. Liao, Y.-S. Chuang, H.-T. Yang, M.-S. Tsai, Bess-sizing optimization for solar PV system integration in distribution grid, IFAC-PapersOnLine 51 (2018) 85–90.

[12] N.B.G. Brinkel, M.K. Gerritsma, T.A. AlSkaif, I. Lampropoulos, A.M. van Voorden, H.A. Fidder, W.G.J.H.M. van Sark, Impact of rapid PV fluctuations on power quality in the low-voltage grid and mitigation strategies using electric vehicles, Int. J. Electr. Power Energy Syst. 118 (2020) 105741.

[13] T. Antić, T. Capuder, M. Bolfek, A comprehensive analysis of the voltage unbalance factor in PV and EV rich non-synthetic low voltage distribution networks, Energies 14 (Dec 2020).

[14] P. González, J. Villar, C.A. Díaz, F.A. Campos, Joint energy and reserve markets: current implementations and modeling trends, Electr. Power Syst. Res. 109 (2014) 101–111.

[15] G. Rancilio, A. Rossi, D. Falabretti, A. Galliani, M. Merlo, Ancillary services markets in Europe: evolution and regulatory trade-offs, Renew. Sustain. Energy Rev. 154 (2022) 111850.

[16] IEA, Tracking clean energy progress 2023, IEA. Licence: CC BY 4.0. 2023. [Online]. Available: https://www.iea.org/reports/tracking-clean-energy-progress-2023.

[17] A. Alsharif, C.W. Tan, R. Ayop, A. Dobi, K.Y. Lau, A comprehensive review of energy management strategy in vehicle-to-grid technology integrated with renewable energy sources, Sustain. Energy Technol. Assess. 47 (2021) 101439.

[18] S. Okhuegbe, C. Mwaniki, M. Akorede, Optimal sizing of hybrid energy systems in a microgrid: a review, in: 2019 Sustainable Research & Innovation Conference, 2019.

[19] X. Luo, J. Wang, M. Dooner, J. Clarke, Overview of current development in electrical energy storage technologies and the application potential in power system operation, Appl. Energy 137 (2015) 511–536.

[20] M. Killer, M. Farrokhseresht, N.G. Paterakis, Implementation of large-scale li-ion battery energy storage systems within the Emea region, Appl. Energy. 260 (2020). 114166, [Online]. Available: https://www.sciencedirect.com/science/article/pii/S0306261919318537.

[21] T. Bocklisch, Hybrid energy storage systems for renewable energy applications, in: Energy Procedia, vol. 73, Elsevier BV, 2015, pp. 103–111. [Online]. Available: https://doi.org/10.1016/j.egypro.2015.07.469

[22] W. Zhuo, A.V. Savkin, Profit maximizing control of a microgrid with renewable generation and bess based on a battery cycle life model and energy price forecasting, Energies 12 (2019) 2904.

[23] I. Worighi, T. Geury, M. El Baghdadi, J. Van Mierlo, O. Hegazy, A. Maach, Optimal design of hybrid PV-battery system in residential buildings: end-user economics, and PV penetration, Appl. Sci. 9 (2019) 1022.

[24] S. Bandyopadhyay, G.R.C. Mouli, Z. Qin, L.R. Elizondo, P. Bauer, Techno-economical model based optimal sizing of pv-battery systems for microgrids, IEEE Trans. Sustain. Energy 11 (2020) 1657–1668.

[25] A. Traore, A. Taylor, M.A. Zohdy, F.Z. Peng, Modeling and simulation of a hybrid energy storage system for residential grid-tied solar microgrid systems, J. Power Energy Eng. 5 (2017) 28–39.

[26] U. Akram, R. Shah, N. Mithulananthan, Hybrid energy storage system for frequency regulation in microgrids with source and load uncertainties, IET Gener. Transm. Distrib. 13 (2019) 5048–5057.

[27] S. Hajiaghasi, M.M. Hosseini Ahmadi, P. Goleij, A. Salemnia, M. Hamzeh, Hybrid energy storage sizing based on discrete Fourier transform and particle swarm optimization for microgrid applications, Int. Trans. Electr. Energy Syst. 31 (2021).

[28] F. Ni, Z. Zheng, Q. Xie, X. Xiao, Y. Zong, C. Huang, Enhancing resilience of DC microgrids with model predictive control based hybrid energy storage system, Int. J. Electr. Power Energy Syst. 128 (2021) 106738.

[29] F. Rassaei, W.-S. Soh, K.-C. Chua, Demand response for residential electric vehicles with random usage patterns in smart grids, IEEE Trans. Sustain. Energy 6 (2015) 1367–1376.

[30] F. Rasaei, W.-S. Soh, K.-C. Chua, Distributed scalable autonomous market-based demand response via residential plug-in electric vehicles in smart grids, IEEE Trans. Smart Grid 9 (2018) 3281–3290.

[31] M.P. Fanti, A.M. Mangini, M. Roccotelli, W. Ukovich, Optimal energy management integrating renewable energy, energy storage systems and electric vehicles, in: 2017 IEEE 14th International Conference on Networking, Sensing and Control (ICNSC), 2017.

[32] M.H.K. Tushar, A.W. Zeineddine, C. Assi, Demand-side management by regulating charging and discharging of the EV, ESS, and utilizing renewable energy, IEEE Trans. Ind. Inf. 14 (2018) 2671–2679.

[33] T. Wakui, K. Sawada, R. Yokoyama, H. Aki, Predictive management for energy supply networks using photovoltaics, heat pumps, and battery by two-stage stochastic programming and rule-based control, Energy 179 (2019) 1302–1319.

[34] D. Coppitters, W. De Paepe, F. Contino, Robust design optimization of a photovoltaic-battery-heat pump system with thermal storage under aleatory and epistemic uncertainty, Energy 229 (2021) 120692.

[35] Q. Yan, B. Zhang, M. Kezunovic, Optimized operational cost reduction for an EV charging station integrated with battery energy storage and PV generation, IEEE Trans. Smart Grid 10 (2019) 2096–2106.

[36] M. Blonsky, P. Munankarmi, S.P. Balamurugan, Incorporating residential smart electric vehicle charging in home energy management systems, in: 2021 IEEE Green Technologies Conference (GreenTech), IEEE, 2021.

[37] P. Huang, M. Lovati, X. Zhang, C. Bales, S. Hallbeck, A. Becker, H. Bergqvist, J. Hedberg, L. Maturi, Transforming a residential building cluster into electricity prosumers in Sweden: optimal design of a coupled pv-heat pump-thermal storage-electric vehicle system, Appl. Energy. 255 (2019) 113864.

[38] M. Yousefi, A. Hajizadeh, M.N. Soltani, B. Hredzak, Predictive home energy management system with photovoltaic array, heat pump, and plug-in electric vehicle, IEEE Trans. Ind. Inf. 17 (1) (2021) 430–440.
[39] G. Stamatellos, O. Zogou, A. Stamatelos, Interaction of a house's rooftop PV system with an electric vehicle's battery storage and AIR source heat pump, Solar 2 (2) (2022). 186–214, [Online]. Available: https://doi.org/10.3390/solar2020011
[40] J.R. Nelson, N.G. Johnson, Model predictive control of microgrids for real-time ancillary service market participation, Appl. Energy 269 (2020) 114963.
[41] M.H. Imani, M.J. Ghadi, S. Ghavidel, L. Li, Demand response modeling in microgrid operation: a review and application for incentive-based and time-based programs, Renew. Sustain. Energy Rev. 94 (2018) 486–499.
[42] V.S. Tabar, S. Ghassemzadeh, S. Tohidi, Energy management in hybrid microgrid with considering multiple power market and real-time demand response, Energy 174 (2019) 10–23.
[43] W. Vermeer, G.R.C. Mouli, P. Bauer, Optimal sizing and control of a pv-ev-bes charging system including primary frequency control and component degradation, IEEE Open J. Ind. Electron. Soc. 3 (2022) 236–251.
[44] M. Gomez-Gonzalez, J.C. Hernández, P.G. Vidal, F. Jurado, Novel optimization algorithm for the power and energy management and component sizing applied to hybrid storage-based photovoltaic household-prosumers for the provision of complementarity services, J. Power Sources 482 (2021) 228918.
[45] C. Zhou, P. Wang, T. Bao, S. Yao, Y. Tang, P. Yang, Flexible load optimal regulation strategy of commercial buildings under the environment of electricity market, Energy Rep. 9 (2023) 1705–1716, [Online]. Available: https://doi.org/10.1016/j.egyr.2023.04.173
[46] A.G. Papakonstantinou, G.N. Psarros, S.A. Papathanassiou, Frequency regulation in island grids with battery storage participating in automatic generation control, in: The 12th Mediterranean Conference on Power Generation, Transmission, Distribution and Energy Conversion (MEDPOWER 2020), IEEE, 2020, pp. 84–89, https://doi.org/10.1049/icp.2021.1220
[47] A. Mohamed, R. Rigo-Mariani, V. Debusschere, L. Pin, Stacked revenues for energy storage participating in energy and reserve markets with an optimal frequency regulation modeling, Appl. Energy 350 (2023). 121721, [Online]. Available: https://doi.org/10.1016/j.apenergy.2023.121721
[48] L. Maeyaert, L. Vandevelde, T. Döring, Battery storage for ancillary services in smart distribution grids, J. Energy Storage 30 (2020) 101524, [Online]. Available: https://doi.org/10.1016/j.est.2020.101524
[49] N. Damianakis, G.R.C. Mouli, Y. Yu, P. Bauer, Coordinated power control of PV generation, electric mobility and electric heating in different grids, in: 2024 IEEE 10th International Power Electronics and Motion Control Conference (IPEMC2024-ECCE Asia), 2024, pp. 2082–2087.
[50] Y. Ding, Y. Zhu, Q. Wang, Z. Tian, R. Yan, Z. Yan, X. Xia, A comprehensive scheduling model for electric vehicles in office buildings considering the uncertainty of charging load, Int. J. Electr. Power Energy Syst. 151 (2023) 109154.
[51] R. Chemudupaty, T. Hornek, I. Pavić, S. Potenciano Menci, Optimizing trading of electric vehicle charging flexibility in the continuous intraday market under user and market uncertainties, Appl. Energy 381 (2025) 125103.
[52] N. Damianakis, Y. Yu, G.R.C. Mouli, P. Bauer, Impact of uncertainties and price of robustness in receding-horizon EV smart-charging, in: 2024 IEEE 21st International Power Electronics and Motion Control Conference (PEMC), 2024, pp. 1–6.
[53] N. Damianakis, Y. Yu, G.C.R. Mouli, P. Bauer, Frequency regulation reserves provision in EV smart-charging, in: 2023 IEEE Transportation Electrification Conference & Expo (ITEC), 2023, pp. 1–6.
[54] N. Damianakis, G.R. Chandra Mouli, P. Bauer, Risk-averse estimation of electric heat pump power consumption, in: 2023 IEEE 17th International Conference on Compatibility, Power Electronics and Power Engineering (CPE-POWERENG), Jun 2023, pp. 1–6.
[55] Tennet TSO, System balance and price information, 2023, https://www.tennet.org/bedrijfsvoering/Systeemgegevens_uitvoering/Systeembalans_informatie/BalansDeltaplusPrijzen.aspx/PanelTabTable (Accessed December 2023).
[56] N. Damianakis, G.R.C. Mouli, P. Bauer, Y. Yu, Assessing the grid impact of electric vehicles, heat pumps & PV generation in Dutch LV distribution grids, Appl. Energy 352 (2023) 121878, [Online]. Available: https://www.sciencedirect.com/science/article/pii/S0306261923012424.
[57] M. Schimpe, M.E. von Kuepach, M. Naumann, H.C. Hesse, K. Smith, A. Jossen, Comprehensive modeling of temperature-dependent degradation mechanisms in lithium iron phosphate batteries, J. Electrochem. Soc. 165 (2) (Jan 2018) A181.
[58] N. Damianakis, K. Kuresoo, G.R. Chandra-Mouli, Battery storage integration in power systems of pvs, and flexible loads for frequency reserves provision and direct load control, SSRN Electron. J. (2025), [Online]. Available: ssrn.com.